Assessing spatio-temporal variability and trends in modelled and measured Greenland ice sheet albedo (2000-2013)

P. M. Alexander[1,2], M. Tedesco[2,1], X. Fettweis[3], R. S. W. van de Wal[4], C. J. P. P. Smeets[4], and M.R. van den Broeke[4]

[1]{Graduate Center of the City University of New York, 365 5th Ave., New York, NY, 10016 USA}

[2]{City College of New York, City University of New York, 160 Convent Ave., New York, NY, 10031 USA}

[3]{Department of Geography, Université de Liège, Place du 20-Août, 7, 4000 Liège, Belgium}

[4]{Institute for Marine and Atmospheric research Utrecht, Utrecht University, Princetonplein 5, 3584 CC Utrecht, The Netherlands}

Correspondence to: P. M. Alexander (palexander@gc.cuny.edu)

Abstract

Accurate measurements and simulations of Greenland Ice Sheet (GrIS) surface albedo are essential, given the role of surface albedo in modulating the amount of absorbed solar radiation and meltwater production. In this study, we assess the spatio-temporal variability of GrIS albedo (during June, July, and August) for the period 2000-2013. We use two remote sensing products derived from data collected by the Moderate Resolution Imaging Spectroradiometer (MODIS), as well as outputs from the Modèle Atmosphérique Régionale (MAR) regional climate model (RCM) and data from in situ automatic weather stations. Our results point to an overall consistency in spatiotemporal variability between remote sensing and RCM albedo, but reveal a difference in mean albedo of up to ~0.08 between the two remote sensing products north of 70°N. At low elevations, albedo values simulated by the RCM are positively biased with respect to remote sensing products by up to ~0.1 and exhibit

low variability compared with observations. We infer that these differences are the result of a positive bias in simulated bare-ice albedo. MODIS albedo, RCM outputs and in situ observations consistently indicate a decrease in albedo of -0.03 to -0.06 per decade over the period 2003-2013 for the GrIS ablation area. Nevertheless, satellite products show a decline in JJA albedo of -0.03 to -0.04 per decade for regions within the accumulation area that is not confirmed by either the model or in situ observations. These findings appear to contradict a previous study that found an agreement between in situ and MODIS trends for individual months. The results indicate a need for further evaluation of high elevation albedo trends, a reconciliation of MODIS mean albedo at high latitudes, and the importance of accurately simulating bare ice albedo in RCMs.

1 Introduction

Over the past decade, the Greenland Ice Sheet (GrIS) has simultaneously experienced accelerating mass loss (van den Broeke et al., 2009; Rignot et al., 2011) and records for the extent and duration of melting (Tedesco et al., 2008, 2011, 2013; Nghiem et al. 2012). Increased melt over Greenland has been associated with both changes in temperature and an amplifying ice-albedo feedback: increased melting and bare ice exposure reduce surface albedo, thereby increasing the amount of absorbed solar radiation and, in turn, further amplifying melting (Box et al., 2012; Tedesco et al., 2011). Recent studies (van den Broeke et al., 2011; Vernon et al., 2013) also indicate that albedo plays an essential role in the GrIS surface energy balance, and consequently, the surface mass balance (SMB) of those regions where considerable melting occurs. Because of the impact of albedo on the surface energy balance, it is crucial to assess the performance of models that simulate albedo over the GrIS and the quality of albedo estimates from remote sensing or in situ observations. These assessments are pivotal for improving our understanding of the physical processes leading to accelerating mass loss, and for improving projections for the next decades.

Several studies that have investigated GrIS albedo trends and variability have primarily relied on satellite measurements, particularly those collected by the Moderate Resolution Imaging Spectroradiometer (MODIS) (e.g. Stroeve et al. 2005, 2006, 2013; Box et al. 2012). Remote sensing measurements can capture changes at large spatial scales and for long periods, continuously (with the exception of cases when the surface is obscured by clouds). Previous studies have found MODIS albedo products to agree reasonably well with in situ data,

especially with regards to capturing the seasonal albedo cycle and mean seasonal values in regions where variability is small (Stroeve et al., 2005, 2006, 2013), but lower accuracy at high solar zenith angles has been identified (Stroeve et al. 2005, 2006), limiting the periods and locations for which these data can be used. Nevertheless, given their relatively high temporal and spatial resolution, these products are useful for evaluating albedo derived from regional climate models (RCMS). RCMs are an important tool for estimating both current and future changes in the GrIS SMB (Box and Rinke, 2002; Box et al., 2006; Ettema et al., 2009; Fettweis et al., 2007, 2011; Rae et al., 2012, Tedesco and Fettweis, 2012), and the surface albedo schemes employed by these models have a substantial impact on their simulation of the SMB (Rae et al., 2012; van Angelen et al., 2012; Lefebre et al., 2005; Franco et al., 2012).

In this paper, we report the results of an assessment of GrIS albedo spatio-temporal variability and trends for the period 2000-2013. To our knowledge, this is the first time that a multi-tool integrated assessment of albedo over Greenland is presented. We use (1) data from two remote sensing products from the Moderate Resolution Imaging Spectroradiometer (MODIS), the MOD10A1 daily albedo product (Hall et al., 2012) and MCD43A3 16 day albedo product (Schaaf et al., 2002), (2) in situ albedo data from the Greenland Climate Network (GC-Net, Steffen et al., 1996) and Kangerlussuaq-Transect (van de Wal et al., 2005), and (3) outputs from two versions (v2.0 and v3.2) of the Modèle Atmosphérique Régionale (MAR; Fettweis et al., 2013a,b). In order to carry out comparisons between products, MODIS data have been regridded to the MAR model grid in some instances daily data have been averaged over 16 day periods when necessary. The role of potential errors associated with differences in spectral range between satellite and in situ data and cloud cover have been considered and corrected for when possible.

2   Data and Methods

2.1   The MAR model

The Modèle Atmosphérique Régionale (Gallée and Schayes 1994; Gallée, 1997; Lefebre et al., 2003), abbreviated MAR, is a coupled land-atmosphere regional climate model featuring the atmospheric model described by Gallée and Shayes (1994) and the Soil Ice Snow Vegetation Atmosphere Transfer scheme (SISVAT) surface model. SISVAT incorporates the multilayer snow model *Crocus* (Brun et al., 1992), which simulates fluxes of mass and energy

1 between snow layers, and reproduces snow grain properties and their effect on surface albedo.
2 The model setup used here is described in detail by Fettweis (2007). We primarily use a
3 recent version of MAR (v3.2), which features changes to the albedo scheme relative to
4 previous versions (v1 and v2), detailed in Section 2.2, but also examine differences between
5 MAR v3.2 and a previous version, MAR v2.0. MAR v3.2 (v2.0) has been run at a 25 km
6 horizontal resolution for the period 1958-2013 (1958-2012). Both model versions are forced
7 at the lateral boundaries and ocean surface and initialized with 6-hourly reanalysis outputs
8 from the European Centre for Medium-Range Weather Forecasts (ECMWF), using the ERA-
9 40 reanalysis (Uppala et al., 2005) for the period 1958-1978 and the ERA-Interim reanalysis
10 (Dee et al., 2011) for the period 1979-present. Here we focus on the 2000-2013 period for
11 comparison with satellite data. The MAR v3.2 ice sheet mask (which gives the fraction
12 covered by ice for each grid box) and surface elevation are defined using the Greenland
13 digital elevation model of Bamber et al. (2013). MAR v2.0 uses the elevation model of
14 Bamber et al. (2001), and the land surface classification mask from Jason Box
15 (sites.google.com/site/jboxgreenland/datasets).

16 In MAR v3.2, in contrast with MAR v2.0, sub-grid scale parameterizations make it possible
17 to have fractions of different land cover types within a single grid box. Quantities are
18 computed for the sectors within each grid box and a weighted average of these quantities is
19 used to represent the average value for a grid box.

20 For the reader's convenience, we show the mean September 2000 - August 2013 SMB from
21 MAR v3.2 in Fig. 1, along with the equilibrium line dividing positive and negative SMB,
22 together with the locations of the weather stations used in this study. In this study, areas
23 below the mean 2000-2013 equilibrium line as defined by MAR are collectively referred to as
24 the "ablation area", while areas above this line are referred to as the "accumulation area".

2.2 The MAR albedo scheme

26 The basis for the MAR albedo scheme is described in detail by Brun et al. (1992) and Lefebre
27 et al. (2003). MAR snow albedo (α) depends on the optical diameter of snow grains (d),
28 which is in turn a function of other snow grain properties, such as grain size, sphericity and
29 dendricity. In the model, the sphericity, dendricity, and size of snow grains are a function of
30 snowpack temperature, temperature gradient, and liquid water content. Albedo is defined in
31 MAR for three spectral intervals:

1   Interval 1, visible (0.3 – 0.8 μm): $\alpha_1 = \max(0.94, 0.96 - 1.58\sqrt{d})$ (1)

2   Interval 2, near infrared (0.8 – 1.5 μm): $\alpha_2 = 0.95 - 15.4\sqrt{d}$ (2)

3   Interval 3, far infrared (1.5 – 2.8 μm): $\alpha_3 = 364 * \min(d, 0.0023) - 32.31\sqrt{d} + 0.88$ (3)

4   where α_1, α_2, and α_3 are wavelength dependent albedo values. The integrated snow albedo

5   (α_S) for the range 0.3 to 2.8 μm is a weighted average of albedo over these intervals based on

6   solar irradiance fractions:

7    $\alpha_S = 0.580\alpha_1 + 0.320\alpha_2 + 0.1\alpha_3$ (4)

8   The minimum albedo of snow is set to 0.65. In MAR v2.0, bare ice albedo was simply

9   assigned a fixed value. In MAR v3.2 (the version primarily used here), bare ice albedo is a

10   function of accumulated surface water following the parameterizations of Lefebre et al.

11   (2003), described below. In the case of bare ice (which occurs in MAR when the surface

12   snow density is greater than 920 kg m^{-3}) ice albedo (a_I) is given by:

13   $\alpha_I = \alpha_{I,min} + (\alpha_{I,max} - \alpha_{I,min})e^{-\left(\frac{M_{SW}(t)}{K}\right)}$ (5)

14   Where $\alpha_{I,min}$ and $\alpha_{I,max}$ are the minimum and maximum bare ice albedo, K is a scale factor (set

15   to 200 kg/m^2), and $M_{SW}(t)$ is the time-dependent accumulated amount of excessive surface

16   meltwater before runoff (in kg m^{-2}). According to the parameterization of Zuo and Oerlemans

17   (1996), there is delay in MAR v3.2 between the production of meltwater and evacuation

18   towards the oceans (Lefebre et al., 2003), in order to account for the reduction of bare ice

19   albedo due to the presence of surface water. The ice surface albedo (α_I) will therefore be

20   lower if the melt rate is higher, asymptotically approaching the minimum bare ice albedo.

21   Additionally, to ensure temporal continuity in simulated albedo, values of albedo between the

22   maximum bare ice and minimum snow albedo are possible when the surface (or near-surface)

23   snow density lies between 830 and 920 kg m^{-3}. In this case (which corresponds to the

24   presence of firn), albedo (α_I) is a function of density as follows (Lefebre et al., 2003):

25   $\alpha_I = \alpha_{I,max} + (\alpha_{S,min} - \alpha_{I,max})\left(\frac{\rho_I - 920 kgm^{-3}}{\rho_C - 920 kgm^{-3}}\right)$ (6)

26   where $\alpha_{S,min}$ is the minimum albedo of snow, ρ_I is the density of the upper firn layer, and ρ_C is

27   the density at which pores within firn close off (830 kg m^{-3}). For the reader's convenience,

1   Table 1 provides the range of possible albedo values for ice, firn, and snow in MAR v2.0 and

2   v3.2.

3   In cases where there is a snowpack with a thickness of <10 cm overlaying ice or firn (with a

4   density greater than 830 kg m^{-3}), excluding the case of ice lenses, albedo is interpolated

5   between the ice albedo and the surface snow albedo as a linear function of snowpack

6   thickness, to produce an "integrated" surface albedo of snow, ice and water (α_{SI}):

7    $$\alpha_{SI} = \alpha_I + \alpha_S(H_S/0.1) \tag{7}$$

8   where H_s is the snowpack height in meters. In cases where a snowpack thicker than 0.1 m lies

9   above ice, or there is bare ice at the surface, α_{SI} is simply set equal to the snow albedo (α_s), or

10   bare-ice albedo (α_I), respectively.

11   **2.3   Satellite-derived albedo**

12   We use the daily MODIS albedo product (MOD10A1, Version-5) distributed by the National

13   Snow and Ice Data Center (Hall et al., 2012; available at http://nsidc.org/data/mod10a1.html),

14   available for the period March 2000 - present, and the 16-day (MCD43A3, Version-5)

15   product from Boston University (Schaaf et al., 2002; available at https://lpdaac.usgs.gov/),

16   available for the same period.

17   The MOD10A1 Version-5 product contains daily albedo (0.3 - 3 µm) based on the "best"

18   daily MODIS observation, defined as the observation that covers the greatest percentage of a

19   grid cell. Corrections are also applied to account for anisotropic scattering, for the influence

20   of the atmosphere on surface albedo, and for the limited spectral range of MODIS bands

21   (Klein and Stroeve, 2002; Stroeve et al., 2006). Here we use MODIS data from the TERRA

22   satellite, as MODIS data from the AQUA satellite are less reliable due to an instrument failure

23   in the near infrared band (Stroeve et al., 2006; Box et al., 2012).

24   The MCD43A3 Version-5 product makes use of all atmospherically-corrected MODIS

25   reflectance measurements over 16-day periods to provide an integrated albedo measurement

26   every 8 days. A semi-empirical bidirectional reflectance function (BRDF) model is used to

27   compute bi-hemispherical reflectance as a function of these reflectance measurements (Schaaf

28   et al., 2002).   The MCD43A3 product contains, in addition to albedo values for each MODIS

29   instrument band, "shortwave" albedo values calculated over a wavelength interval of 0.3-5.0

30   µm and "visible" albedo values for the 0.3-0.7 µm interval, calculated using the BRDF

1 parameters. Here we primarily make use of "shortwave" MCD43A3 albedo, as its

2 wavelength interval is consistent with those of MAR and MOD10A1, but briefly consider

3 "visible" albedo as well. The MCD43A3 product provides, over each wavelength interval, an

4 integrated diffuse White Sky Albedo (WSA) and a direct Black Sky Albedo (BSA) for a

5 specific viewing geometry (from above when the local solar zenith angle is at a maximum).

6 A linear combination of WSA and BSA can be used to compute the true "blue-sky albedo".

7 Stroeve et al. (2005) suggest that there is little difference between BSA and WSA for typical

8 summer midday solar zenith angles over Greenland. Simulation of blue-sky albedo requires

9 models or observations of aerosol optical depth (e.g. Stroeve et al., 2013) that are not

10 available for this study and therefore, the following results consider BSA only.

11 Both MODIS products provide quality flags indicating "good quality" vs. "other quality"

12 data. In the case of MCD43A3, "other quality" data are produced using a "backup"

13 algorithm. When few observations are available, the backup algorithm is used to scale an

14 archetypal BRDF function that is based on past observations (Schaaf et al., 2002). In order to

15 understand the influence of data quality on our results, we present results for both "all

16 quality" as well as "good quality" data.

2.4 Weather station data

18 We use Automatic Weather Station (AWS) data from two sources, the Greenland Climate

19 Network (GC-Net, Steffen et al., 1996) and the Kangerlussuaq Transect (K-Transect, van de

20 Wal et al., 2005). The locations of the weather stations are shown in Fig. 1, and a list of the

21 weather stations used and their period of coverage is provided in Table 2. We use all

22 available GC-Net and K-transect June-July-August (JJA) data within the period 2000-2012

23 for comparison with MODIS and MAR albedo. (GC-Net data for the summer of 2013 were

24 not yet available when data analysis for this study was conducted.) We follow a procedure

25 similar to that employed by Stroeve et al. (2005) to generate albedo timeseries' from GC-Net

26 and K-Transect data. Mean daily albedo was computed as the sum of daily incident

27 shortwave (SW) radiation divided by the sum of daily outgoing SW radiative flux. Instances

28 where hourly upward SW radiative flux exceeds downward SW radiative flux were excluded.

29 Upward and downward hourly radiative fluxes were excluded when downward fluxes were

30 smaller than 250 W/m^2 to reduce the impact of relative errors on measured albedo, especially

31 during cases of low incident radiation. (We investigated the sensitivity of our results to this

32 threshold, and did not find a considerable effect on the results). Data from several locations

1 and time periods were excluded from this analysis. These stations are included in Table 2. In

2 particular, measured albedo at Swiss Camp for the year 2012 appeared to be unrealistically

3 high relative to previous years and was excluded (mean measured JJA albedo for 2012 was

4 0.99, 3.5 standard deviations above the mean 2000-2011 value of 0.64). Measured albedo at

5 Crawford Point-2 undergoes a step change after 2004 (mean albedo is 0.81 ± 0.03 for 2000-

6 2004 and 0.90 ± 0.04 for 2005-2010) and therefore we excluded data after 2004, as was done

7 by Stroeve et al. (2013). At the stations NASA-U and NGRIP, leveling errors produce a low

8 bias in upward radiation for all years (Stroeve et al., 2013) resulting in measured albedo

9 values that are unrealistically low for snow outside of the ablation area (0.30 ± 0.01 at NASA-

10 U and 0.33±0.01 at NGRIP), and are therefore excluded. At the Peterman Glacier and

11 Peterman ELA, missing MODIS data prevented us from including all weather station data in

12 this analysis.

13 **2.5 Methods of analysis**

14 2.5.1 Corrections to MAR albedo

15 Snow albedo is generally higher during cloudy conditions due to the masking of a portion of

16 the incoming solar spectrum by clouds (Greuell and Konzelman, 1994). Both MAR v3.2 and

17 MAR v2.0 account for this factor by applying a correction to the integrated surface albedo

18 (α_{SI}) as a function of cloud fraction, following Greuell and Konzelman (1994):

19 $$\alpha_{CL} = \alpha_{SI} + 0.05(n - 0.5) \qquad (8)$$

20 where n is the cloud fraction computed by MAR, and α_{CL} is the cloud-corrected albedo.

21 Satellite data can only provide cloud-free measurements, and therefore we re-correct MAR

22 surface albedo to produce estimates of cloud-free surface albedo. We use this particular

23 technique rather than excluding pixels from MAR because MAR does not necessarily

24 replicate the actual cloud fraction observed by MODIS. The correction applied here reverses

25 the correction applied in MAR, then corrects albedo for the case where there is a cloud

26 fraction of 0:

27 $$\alpha_{MAR,clear-sky} = \alpha_{MAR,daily} - 0.05(n_{MAR,daily} - 0.5) - 0.025 \qquad (9)$$

28 In this case $\alpha_{MAR,\ daily}$ is the daily mean MAR albedo, $n_{MAR,\ daily}$ is the daily mean cloud

29 fraction from MAR, and $\alpha_{MAR,\ clear-sky}$ is the daily mean clear-sky albedo. All analyses with

30 MAR results are conducted using $\alpha_{MAR,\ clear-sky}$.

2.5.2 Aggregation of MODIS data to the MAR grid

For the purpose of comparing model results and satellite data, MODIS albedo products are re-gridded to the MAR 25 km resolution grid from the original 463 m spatial resolution at which they are distributed. Re-gridded values contain the median value of all the MODIS values falling within a MAR grid box. When comparing satellite datasets and satellite data against model results, we restrict our analysis to the GrIS. For all comparisons including MAR v3.2 results, areas where the MAR sub-grid level ice cover percentage is less than 100% are excluded. For all comparisons including MAR v2.0 results, the same mask from MAR v3.2 is used, except that pixels classified as 100% ice covered in MAR v3.2, but classified as non-ice-covered in MAR 2.0 are also excluded from the analysis.

2.5.3 Comparisons at in situ stations

Comparisons at in situ stations are conducted between weather station data and data or outputs from the MODIS or MAR grid box that encompasses the in situ station. In this case we use the original (463x463m) MODIS grid box containing the station rather than the MODIS data aggregated to the encompassing 25x25 km MAR grid box to reduce potential errors associated with spatial variations of albedo. In cases where an in situ station is contained within a MAR grid box classified as less than 100% ice-covered in MAR v3.2, we compare in situ data to MAR v3.2 data from the ice-covered sector of that grid box rather than data from the entire grid box.

As in the case of the original MAR albedo outputs, in situ measurements also include measurements made during cloudy conditions while MODIS albedo data do not. Given a lack of available measurements, we do not explicitly correct in situ data for the presence of clouds in this study, but only consider data where coincident satellite and in situ measurements are available. Stroeve et al. (2013) applied a correction to GC-Net data using a radiative transfer model, but found that the correction did not significantly impact their results.

2.5.4 Spectral differences

The GC-Net LI-COR sensors are sensitive within the 0.4-1.1μm band, and K-Transect data are collected in the 0.3-2.8 μm band. The GC-Net bands are narrower than the MOD10A1 interval of 0.3-3μm and the MCD43 shortwave albedo interval of 0.3-5μm, and the interval of 0.3-2.8μm over which albedo is calculated in the MAR model. GC-Net incoming and

1   outgoing radiation values are calibrated to represent radiation for a spectral interval of 0.28 to

2   2.8 μm (Wang and Zender, 2009). However, because snow has a high spectral reflectance

3   over the 0.3 to 1.1 μm interval, and a much lower reflectance above 1.1 μm, measured albedo

4   over the smaller interval will be higher for snow-covered areas (Stroeve et al., 2005). Stroeve

5   et al. (2005) compared albedo derived with GC-Net LI-COR pyranometers to measurements

6   from pyranometers with a larger spectral range, and found that the smaller wavelength

7   interval results in a positive albedo bias of between 0.04 and 0.09, for GC-Net data relative to

8   MODIS albedo, depending on the location and time period (Stroeve et al., 2005). This bias

9   does not apply to K-Transect measurements, as the spectral sensitivity is comparable to the

10   sensitivity of MODIS sensors. Because this bias may be smaller or larger depending on

11   multiple factors, we do not apply any correction here, but provide an indication of spatial

12   variability of this bias in Section 4.2.1 by comparing MCD43A3 visible albedo (0.3 – 0.7 μm)

13   with MCD43A3 shortwave (0.3-5.0 μm) albedo.

14   2.5.5 Calculation of bias, correlation, and trends

15   In the following analysis, we focus on the JJA period because MODIS data are less reliable

16   during other months, when solar zenith angles are high, as discussed by Box et al. (2012), and

17   because this is the period when surface albedo has the largest impact on SMB.

18   In order to compare spatial variations in albedo we calculated the mean 2000-2013 JJA

19   MOD10A1, shortwave MCD43A3 BSA albedo, and MAR clear-sky albedo using all

20   available measurements or model outputs over the specified period, excluding cases where

21   greater than 25% of data were missing for a given pixel. When differences between datasets

22   or between satellite data and model results are calculated, we only use measurements or

23   results that overlap in time and space, to avoid the possibility of biases introduced by missing

24   data. The mean difference between two samples for a given grid box was deemed to be

25   statistically significant if the p-value for a two-sample Student's t-test was smaller than 0.05.

26   Unless otherwise specified, we use only "good quality" MODIS data in comparisons.

27   In some cases, observational data or model results have been spatially averaged or aggregated

28   within the ablation and accumulation areas defined using MAR v3.2 or v2.0. The ablation

29   (accumulation) area is defined as the area that experienced a net loss (gain) of mass over the

30   2000-2013 period as simulated by either version of the model.

For analyses of temporal variability, we consider daily variability, for which MOD10A1 data, in situ values, and MAR outputs available, as well as variability over 16-day MCD43A3 periods. In the case of the analysis of 16-day data, MOD10A1, MAR, and in situ daily data are averaged to produce a value for each overlapping MCD43A3 16-day period. We examine the correlation between daily satellite data and between satellite data and model results using Pearson's coefficient of determination (r^2).

To compare the distribution of ablation area albedo for satellite data and MAR model outputs, we produced frequency histograms for ablation area albedo using a bin width of 0.0099. Parameters for the best fit of a bimodal distribution to the histograms was obtained using the maximum likelihood estimation function in MATLAB, assuming a bimodal normal distribution for the fit.

Box et al. (2012) investigated changes in GrIS albedo using the MOD10A1 albedo product, finding that between 2000 and 2012, surface albedo decreased over almost the entire ice sheet. Here, we build on the analysis of Box et al. (2012) and extend the analysis to include MCD43A3, MAR v3.2 and in situ JJA data for the period 2000-2013. Trends in albedo have been obtained by performing linear regression on 16-day albedo values for satellite products, in situ data, and model outputs, excluding albedo values outside of the JJA period. We have also computed trends for annual JJA average values. A trend was determined to be statistically different from 0 if the p-value for a Student's t-test was smaller than 0.05. For in situ stations, only stations with a record of at least 9 years of data are included in the analysis, and only trends for albedo from the encompassing MAR v3.2 (25x25 km) grid box and MODIS (463x463m) grid boxes over the same range of years are considered.

3   Results

3.1   Albedo spatial variability

MAR v3.2 and the two MODIS datasets show coherent spatial patterns of JJA mean 2000-2013 albedo (Fig. 2) that are consistent with previous studies (e.g., Box et al., 2012), with low-elevation areas in the ablation area dominated by lower albedo values (<0.7 on average, Table 3) due to the presence of meltwater and bare ice, and high elevation areas by relatively higher albedo (>0.74). The most obvious discrepancy between the satellite products occurs north of 70°N, where the MOD10A1 daily product exhibits an increase in albedo with

1 latitude, while MCD43A3 points to the opposite. The difference between the two satellite

2 products (Fig. 3a) is statistically significant (at the 95% confidence level) above 70°N,

3 reaching ~0.08 (for albedo ranging between 0 and 1) at the highest latitudes.

4 The pattern of differences between MAR v3.2 and the two satellite products (Fig. 3b and c)

5 appears to vary with both elevation and latitude, while the difference between the two satellite

6 products varies primarily with latitude (Fig. 3a). Because any systematic biases in the

7 satellite products are likely to be relatively consistent across space (at least as a function of

8 longitude), it is likely that MAR v3.2 biases contribute to some of the elevational differences

9 seen in Figs. 3b and c. Within the accumulation area south of 70°N, MAR v3.2 albedo (0.77

10 on average) is comparable to MODIS albedo (average of 0.78 for MOD10A1 and 0.77 for

11 MCD43A3). At low elevation areas, especially along the west coast ablation area, MAR v3.2

12 overestimates albedo (up to ~0.1) relative to both satellite products. The mean ablation area

13 albedo from MOD10A1 (0.68 ± 0.07) is identical to MAR mean ablation area albedo (Table

14 3), despite the large positive bias in MAR albedo within the west coast ablation area that can

15 be seen in Fig. 3. This is likely a result of a positive bias for MOD10A1 at high latitudes, as

16 will be discussed further below. For areas north of 70°N, the discrepancy between satellite

17 products makes it impossible to determine the magnitude and direction of MAR biases.

18 MAR v3.2, MOD10A1 and MCD43A3 mean 2000-2013 JJA albedo values show a similar

19 logarithmic dependence of albedo with elevation (Fig. 4a); below 2000 m, albedo increases

20 relatively rapidly with elevation (both MAR and the MODIS products show a statistically

21 significant albedo increase of ~0.01 to ~0.02 per 100 m increase in elevation), while above

22 2000 m, the change is smaller (no statistically significant increase for MAR, and an increase

23 of ~0.002 to ~0.003 per 100 m for both MODIS products). The discrepancies between

24 MODIS products north of 70°N are evident in Fig. 4b: MCD43A3 decreases with latitude

25 while MOD10A1 increases, and MAR v3.2 shows little change.

26 For in situ stations in the ablation area (Table 4), in situ mean albedo (0.56 ± 0.08) is higher

27 than coincident average MOD10A1 (0.51 ± 0.09) and MCD43A3 (0.50 ± 0.07) albedo values,

28 and is comparable with MAR v3.2 clear sky mean albedo for sectors classified as ice-covered

29 (0.57 ± 0.07). Within the accumulation area, in situ albedo is larger by 0.01 to 0.06 relative to

30 MAR and the MODIS products (Table 4). These results appear to be consistent with a

31 positive bias in GC-Net measurements identified by Stroeve et al. (2005). However, we also

32 find that the difference between in situ and satellite albedo is larger at K-Transect stations

1   (+0.08) than at GC-Net sites (+0.04), and K-Transect data are not expected to exhibit the

2   positive bias. It is likely that the high spatial variability of ablation area albedo contributes to

3   the differences. Data from in situ stations may be positively biased relative to satellite data

4   because of a bias introduced by station locations: locations are not chosen to be within

5   streams, lakes, or crevasses, which have a lower albedo. In the acccumulation zone, a lack of

6   variation in surface features likely leads to smaller spatial variations in albedo.

7   Mean 2000-2012 JJA albedo values for ablation area GC-Net stations with a record of at least

8   7 years does not appear to exhibit a clear variation with latitude when compared with satellite

9   data and model results (Fig. 5). GC-Net albedo at stations north of 70°N is on average larger

10 by 0.02 relative to stations south of 70°N (Table 4), suggesting that GC-Net albedo does not

11 confirm the decrease in albedo with latitude indicated by MCD43A3. MOD10A1

12 accumulation area measurements are comparable (within 0.01 for aggregated station data) to

13 uncorrected GC-Net data north of 70°N (Fig. 5, Table 4). This suggests that the MOD10A1

14 may also be positively biased north of 70°N.

15 It appears possible from Fig. 5 that the bias at GC-Net sites (between 0.04 and 0.09 according

16 to Stroeve et al., 2005) could increase with latitude, rendering corrected GC-Net mean 2000-

17 2013 albedo comparable to MCD43A3 albedo. In order to indicate how the GC-Net albedo

18 bias is likely to vary spatially, the mean difference between MCD43A3 visible BSA (for the

19 interval 0.3-0.7 μm) and MCD43A3 shortwave BSA (for the interval 0.3-5.0 μm) was

20 computed (Fig. 6). The difference is larger than the biases observed by Stroeve et al. (2005)

21 at GC-Net stations likely because the MCD43A3 visible wavelength interval is smaller than

22 that for GC-Net stations. The difference does not vary with latitude, but is rather lowest in

23 the ablation area, where bare ice is exposed during summer months, is largest in regions

24 where melting occurs, but bare ice exposure is infrequent, and is relatively small at high

25 elevations.

26 The spatial variability of the difference appears to be associated with the differences in

27 spectral albedo between different materials. Because ice does not exhibit the spectral

28 dependence of albedo that snow does (Hall and Martinec, 1985), the difference between

29 MCD43A3 visible and shortwave albedo is lower in the albation area, where bare ice is

30 exposed during summer. In locations where melting occurs, snow grains tend to be larger

31 because of constructive metamorphism, reducing reflectance mostly in the near infrared band

32 (Wiscombe and Warren, 1980), resulting in a larger difference between visible and near

1 infrared reflectance. This suggests that in situ albedo values do not exhibit the decrease of
2 albedo with latitude suggested by MCD43A3.

3.2 Albedo temporal variability

4 The standard deviation of albedo time-series provides information on the magnitude of its
5 temporal variability. Within the low elevation ablation area of the ice sheet, both MAR and
6 the MODIS products exhibit a relatively high standard deviation for the 2000-2013 period
7 (0.07 on average for 16 day periods; Fig. 7, Table 3). At high elevations, variability is smaller
8 (0.02 to 0.03 on average for 16 day periods). The MCD43A3 and MOD10A1 products show
9 similar spatial patterns of standard deviation when the daily product is averaged over 16 day
10 MODIS periods (Fig. 7a and c). Table 3 suggests that MAR v3.2 ablation area temporal
11 variability is identical to MODIS variability on average, but Fig. 7 shows that there are
12 locations, particularly within the west coast ablation area, where MODIS variability is
13 considerably higher. MAR v3.2 albedo variability in low elevation areas reaches a maximum
14 of 0.09, while MODIS variability for the same regions is 0.15 at maximum. At a daily
15 temporal resolution, MOD10A1 daily variability in the ablation area (0.17 maximum, 0.07 on
16 average) is considerably larger than the variability of MAR v3.2 albedo (0.12 maximum, 0.04
17 on average). As will be discussed in section 4.2, this may be the result of a positive bias in
18 bare-ice albedo from MAR, but may also be associated with errors introduced by cloud
19 artifacts in the MOD10A1 product. For the accumulation area, the standard deviation of
20 albedo for MAR and MODIS generally falls within the 16 day uncertainty of 0.04 for
21 MCD43A3 high-quality albedo and daily uncertainty of 0.067 for MOD10A1 albedo
22 estimated by Stroeve et al. (2005, 2006). This limits the comparison among MAR and the
23 MODIS products for high elevations.

24 For areas south of 70°N and in the ablation area north of 70°N, the two MODIS products are
25 highly correlated (for MCD43A3 16 day periods, $r^2 > 0.5$), but in the accumulation area north
26 of 70°N this correlation decreases (Fig. 8a). Poor correlation in this area is likely a result of
27 the low standard deviation of albedo which falls within the uncertainty range for MODIS.
28 Maps of the coefficient of determination between MAR and MODIS (Fig. 8b and c) indicate
29 that MAR v3.2 captures more than 50% of the ablation area variability detected by satellite
30 products for 16 day periods and more than 25% for daily periods. It is, however, important to
31 note that the daily variability from MOD10A1 is partially driven by cloud artifacts retained in
32 the MOD10A1 product (Box et al., 2012). Again, in the accumulation area, it is difficult to

1   draw any conclusions regarding correlation, as the variability in albedo is smaller than the

2   assumed uncertainty for the MODIS products.

3.3 Albedo spatio-temporal variability

4   Further insights into the consitency of spatio-temporal variations in albedo between MODIS

5   products and between MAR and MODIS products can be drawn from scatter plots for all

6   MCD43A3 vs. MOD10A1 2000-2013 JJA albedo values (Fig. 9a) and MAR vs. MODIS

7   values (Fig. 9b-d). Figure 9a indicates that MCD43A3 albedo is lower (by 0.03 on average)

8   compared to MOD10A1 albedo, consistent with the significant difference between the

9   products at high latitudes seen in Fig. 3a. There is a fairly good correlation between

10   MCD43A3 and MOD10A1 ($r^2 = 0.66$) and the slope of the best linear fit (0.83) is close to 1.

11   When MAR is compared with MCD43A3 and MOD10A1 over 16 day periods (Fig. 9b and

12   c), the correlation between MAR and satellite data is as good or better than the correlation

13   between MOD10A1 and MCD43A3 ($r^2 = 0.66$ vs. MOD10A1 and 0.81 vs. MCD43A3).

14   However, there is less agreement about the 1 : 1 line; a linear fit reveals a slope of 0.58 for

15   MAR vs. MCD43A3 and 0.51 for MAR vs. MOD10A1. MAR overestimates low values of

16   albedo (below 0.6) relative to satellite data, which is consistent with the apparent positive

17   MAR bias in the ablation area seen in Fig. 3b and c. On a daily basis, there is a poor

18   agreement between MAR and MOD10A1 (Fig. 9d, $r^2=0.35$), consistent with the poor

19   correlations observed in Fig 8d. (Note that MOD10A1 albedo is only accurate to two decimal

20   places, resulting in the apparent vertical lines in Fig. 8d.)

21   Scatter plots of 2000-2012 JJA albedo values for both satellite products and MAR v3.2 vs. all

22   weather station measurements (Fig. 10) indicate a strong correlation between in situ data and

23   the two satellite products over 16 day periods (Fig. 10a and b; $r^2 = 0.80$ for MOD10A1,

24   $r^2=0.81$ for MCD43A3), as well as a good agreement about the 1 : 1 line (slope = 0.95 for

25   MOD10A1 and 0.88 for MCD43A3). MAR agrees reasonably well with in situ data, but the

26   correlation is lower ($r^2 = 0.78$), and the slope (0.66) is further from 1. Again, it appears that

27   MAR also overestimates low albedo values relative to in situ measurements, in consistency

28   with Fig. 9b and c.

29   On a daily basis, MOD10A1 albedo exhibits a nearly 1 : 1 relationship with daily in situ

30   albedo (Fig. 10d; slope = 0.99), although there is increased scatter ($r^2=0.75$) due to higher

31   variability on daily timescales (Fig. 7). Similarly, when MAR is compared with daily in situ

1 measurements, the correlation is lower relative to the 16 day comparison (r^2=0.74), while the

2 slope of the best fit line does not change substantially (slope = 0.65).

3 In situ and satellite data and MAR v3.2 outputs all indicate that spatiotemporal variability of

4 albedo is higher in the ablation area (where the standard deviation of albedo is ~0.13) than in

5 the accumulation area (standard deviation of ~0.04). This is to be expected, given that the

6 ablation area undergoes a substantial seasonal cycle in melting.

7 **3.4   MAR v3.2 vs. MAR v2.0 albedo**

8 In order to further examine some of the discrepancies between MAR and observations, we

9 find it useful to examine differences between MAR v3.2 and MAR v2.0, which has been

10 validated against satellite and in situ data (e.g. Fettweis et al., 2005, 2011) and used for

11 making future projections (Fettweis et al., 2013b; Tedesco and Fettweis, 2012). A major

12 difference between MAR v3.2 and MAR v2.0 is in the scheme for calculating the albedo of

13 bare ice; MAR v2.0 bare ice albedo is set to 0.45, while in MAR v3.2, it ranges between 0.45

14 and 0.55 as a function of surface melt (Table 1).

15 Scatter plots for MAR vs. MODIS 2000-2012 JJA albedo in the ablation area, along with

16 frequency histograms and best fit curves of the distribution (Fig. 11) suggest that there is a

17 bimodal distribution of ablation area albedo, which we attribute to the presence of two main

18 surface types, ice (and firn) and snow. Pixels classified by MAR as having bare ice (or firn,

19 surface density > 830 kg m^{-3}) for at least 8 days of each 16 day period coincide with one of

20 the peaks in the bimodal distributions (Fig. 11).

21 There are differences in the observed distributions, however. MAR v2.0 exhibits a clustering

22 of albedo values above 0.65 and below 0.55 (Fig. 11a). MCD43A3 exhibits an overlap in the

23 distribution of the two modes, and there is a wider range of low albedo values (σ=0.10 for

24 MCD43A3 and 0.05 for MAR for the best fit of the lower albedo peak; Table 5). The MAR

25 v3.2 distribution exhibits a slightly wider range of low albedo values (σ=0.06 for the low

26 albedo peak) with a mean that is positively shifted relative to MAR v2.0 (μ=0.61 vs. 0.50)

27 (Fig. 11b). MOD10A1 does not appear to exhibit a bimodal distribution with two distinct

28 peaks, but the best-fit curve agrees qualitatively with the observed distribution (Fig. 11c).

29 The higher uncertainty and therefore increased variability for the MOD10A1 product (Fig. 6;

30 Stroeve et al., 2006) may possibly mask the two peaks of the distribution. Indeed, the best-fit

1   bimodal distribution from MOD10A1 has a higher standard deviation of albedo for the higher

2   albedo peak ($\sigma = 0.06$ for MOD10A1 vs. 0.04 for MCD43A3; Table 5).

3   We compare MAR v2.0 mean 2000-2012 clear-sky JJA albedo with albedo from MAR v3.2

4   and MODIS in Figs. 12a-c. MAR v3.2 albedo is significantly larger in the ablation area

5   compared with MAR v2.0 (Fig. 12a). Rather than being positively biased relative to MODIS

6   (as is the case for MAR v3.2 as shown in Fig. 3), MAR v2.0 albedo is either negatively biased

7   or is not significantly different from MODIS data (Fig. 12b and c). The difference in albedo

8   scheme is the major difference between MAR v3.2 and MAR v2.0, and it results in a

9   significant difference in SMB (Fig. 12d). The average ablation area JJA SMB for MAR v3.2

10   is higher by 0.53 mWE yr^{-1} compared with the average for MAR v2.0, a considerable

11   fraction (roughly 25%) of the mean ablation area JJA SMB from MAR v3.2, which is on

12   average -2.02 mWE/yr for the period 2000-2013. This highlights the importance of a model's

13   albedo scheme in determining the ablation rate and size of the ablation area (van Angelen et

14   al., 2012).

15   **3.5   Greenland Ice Sheet albedo trends**

16   MAR v3.2, MCD43A3, and MOD10A1 consistently agree that there has been a significant

17   decrease in albedo within the ablation area over 2000-2013, and that the largest decreases in

18   albedo have occurred below 2000 m a.s.l. (Figs. 13 and 14). MCD43A3 shows a decrease of

19   up to -0.1 per decade for pixels in the ablation area, as does MOD10A1 (both products show a

20   decrease of -0.06 per decade for the entire area). MAR v3.2 agrees with these trends, but the

21   overall magnitude is smaller (-0.03 per decade for the entire area).

22   Within the accumulation area, MAR v3.2 disagrees with the two MODIS products as to the

23   direction and magnitude of trends. MCD43A3 shows a decrease of -0.03 per decade on

24   average, and MOD10A1 trends are somewhat larger (-0.04 per decade on average), while for

25   MAR v3.2, trends are generally not statistically significant at the 95% level for grid boxes

26   above 2500 m a.s.l., and are slightly positive in some high-elevation areas.

27   For locations within the GrIS ablation area, trends at GC-Net stations with a record of at least

28   9 years are consistent with significant decreases in albedo indicated by MODIS and MAR the

29   periods covered (2000-2012 or 2004-2012; Table 6). The magnitude of the trends varies

30   between MAR v3.2, MODIS and in situ data at individual stations. These differences can be

31   attributed in part to the high spatio-temporal variability of albedo within the ablation area.

This can potentially lead to trends at a weather station that are substantially different from trends within a 500 m MODIS grid box containing the location of that weather station. At higher elevations, this factor is less important as there is less spatio-temporal variability in albedo (Figs. 9 and 10). Within the accumulation area, trends at weather stations are generally within ±0.01 per decade of MAR trends; they are generally not statistically significant and are close to zero, unlike MODIS estimates, which show trends ranging between -0.01 and -0.07 per decade (Table 6).

4   Discussion

4.1   Albedo properties of the Greenland Ice Sheet common to all observations and model results

The results presented above highlight certain features of Greenland ice sheet albedo variability that are common to in situ, satellite data, and model results. MAR, MODIS and in situ data capture general spatial patterns of low albedo in the ablation area, which increases with increasing elevation below ~2000 m and is relatively insensitive to elevation at higher elevations (Figs. 2 and 4a, Table 4). This spatial variability is consistent with the presence of meltwater and bare ice exposure at low elevations, which are a function of surface air temperatures, and therefore elevation (Tedesco et al., 2011; Fettweis et al., 2011). Bare ice in the ablation area is often covered with dust, further reducing low elevation albedo (Bøggild et al., 2010; Wientjes and Oerlemans, 2010; Wientjes et al., 2011). At high-elevation areas that are permanently snow covered, particularly at northern sites, melting is infrequent (Nghiem et al., 2012; Tedesco et al., 2011) and albedo variability is primarily associated with accumulation, subsequent dry snow grain size metamorphism (Wiscombe and Warren, 1980), and possibly impurities (Dumont et al., 2014). Low elevation melting and bare ice exposure during warm summer months reduces surface albedo relative to snow albedo, resulting in a seasonal cycle that increases local variability. As Fig. 7 and Tables 3 and 4 show, there is higher variability in ablation area albedo (where the mean standard deviation of albedo at in situ stations ranges between ±0.06 and ±0.09) relative to the accumulation area (where standard deviations range between ±0.02 and ±0.04).

As noted in Section 3.5, MAR, MODIS, and in situ data agree that there has been a significant decline in ablation area albedo between 2000 and 2013. These trends in surface albedo are

1 associated with increased melting and bare ice exposure resulting in a declining ablation area

2 SMB, captured by models (Fettweis et al., 2011; Ettema et al., 2009) and in situ observations

3 (van de Wal et al., 2012). Increased melting has been linked to higher regional atmospheric

4 air temperatures, associated with atmospheric circulation changes (Fettweis et al., 2013a;

5 Häkkinen et al., 2014).

6 4.2 Insights from differences between datasets

7 4.2.1 Variation of albedo with latitude

8 Results from sect. 4.1 indicate that above 70°N, MOD10A1 shows an increase in albedo with

9 latitude, MCD43A3 exhibits a decrease, MAR shows little change, and there is also a small

10 increase with latitude at local weather stations (Figs. 2, 4b, 5, Table 4). The increase with

11 latitude at local stations is likely unaffected by differences in spectral range between MODIS

12 and in situ sensors (Fig. 10).

13 Theoretically, snow albedo is expected to increase with increasing solar zenith angle,

14 particularly for high solar zenith angles (Wiscombe and Warren, 1980) and therefore will

15 increase slightly with latitude at high latitudes, as long as other factors do not contribute to

16 lower albedo values. Wang and Zender (2009) compared 16 day MCD43C3 albedo with GC-

17 Net measurements and suggest that the MCD43C3 product is unrealistic at higher latitudes, in

18 particular for solar zenith angles > 55°. (The MCD43C3 product differs from the MCD43A3

19 product used here only in its grid.) Schaaf et al. (2011) and Stroeve et al. (2013) suggest that

20 the findings of Wang and Zender (2009) are inaccurate, partially because they did not separate

21 results for high- vs. low-quality albedo. We have considered this in our study: results for all

22 MCD43A3 data are shown along with good quality MCD43A3 data in Fig. 4b. While the use

23 of only good quality data increases MCD43A3 albedo above 70°N, it does not fundamentally

24 change the dependency of MCD43A3 albedo on latitude. For MOD10A1, excluding low

25 quality data has little effect on the binned values.

26 It should also be noted that the MOD10A1 product, to the contrary, may be positively biased

27 above 70°N, given that it is comparable with uncorrected GC-Net data, which are likely

28 positively biased (Fig. 5). We do not have a reasonable explanation for this potential bias, but

29 as noted by Box et al. (2012), the MOD10A1 product contains artifacts that have not been

30 removed during quality control, even for "good quality" data. The in situ observations of

31 Konzelmann and Omura (1995) also suggest that values of albedo above 0.84 are unrealistic

1 for snow under clear-sky conditions. Part of the reason for discrepancies in the latitudinal

2 dependence of albedo may be associated with biases resulting from viewing geometry or sun

3 angle, which vary with latitude, making it difficult to draw conclusions from the various

4 observational datasets as to "true" variations in albedo with latitude.

5 **4.2.2 Differences between MAR v3.2, MAR v2.0 and observations**

6 The major difference between MAR v3.2 albedo and observed albedo is an overall positive

7 bias in the ablation area. This bias can be seen most clearly as a difference of ~0.1 between

8 MAR v3.2 and the two MODIS products along the west coast ablation area in Fig. 3b and c,

9 and in a difference between MAR v3.2 and both MODIS products of 0.06 at in situ stations

10 (with low elevation stations mostly located in the west coast ablation area). Mean ablation

11 area albedo from local stations is also comparable with coincident MAR v3.2 albedo (Table

12 4), but local station measurements are likely positively biased, further confirming a positive

13 MAR bias in this area.

14 Scatter plots of ablation area albedo appear to confirm this: when MAR v3.2 is compared

15 with both MODIS data and in situ measurements (Figs. 9b, c and 10c) the result is a best fit

16 line with a slope smaller than one. Additionally in the same area where MAR v3.2 appears

17 positively biased in the west coast ablation area, MODIS exhibits relatively high variability

18 compared with MAR v3.2 (as discussed in Sect. 3.3; Fig. 7).

19 Biases in MAR ablation area albedo are related to its ability to capture the observed bimodal

20 distribution in ablation zone albedo (Fig 11) associated with two main surface types, ice and

21 snow. The positive bias from MAR v3.2, as well as the relatively low modeled variability in

22 the ablation area is the result of the albedo values set for bare ice in MAR v3.2 (Table 1) that

23 may be too high on average. MAR v2.0 albedo, by contrast, which has a fixed bare ice albedo

24 of 0.45, generally exhibits a negative bias in most portions of the ablation zone. A bare ice

25 albedo that is too high will also lead to a smaller difference between the albedo values of

26 melting snow and bare ice, reducing temporal variations in ablation area albedo, resulting in

27 the relatively low variability from MAR v3.2 (Fig. 7).

28 An examination of Fig. 11 indicates that the low albedo peak for MAR v3.2 is closer to being

29 normally distributed compared with the peak for MAR v2.0, and therefore better matches the

30 distribution from MCD43A3. However, the MAR v3.2 parameterization overestimates the

31 bare ice albedo, as already discussed, and still does not fully capture the variability in the low

albedo peak for MODIS albedo (σ=0.06 for MAR v3.2 and σ=0.10 for both MODIS products). The results suggest that although MAR v3.2 appears to correct a low albedo bias present in MAR v2.0, and introduces a somewhat more realistic distribution of albedo in the ablation area, it also introduces a positive albedo bias, particularly along the west coast ablation zone, which is rich in impurities.

MAR albedo is only a function of accumulated meltwater and does not explicitly take into account the presence of dust, surface lakes and surface streams, including the West Greenland "dark zone" (van de Wal and Oerlemans, 1994; Wientjes and Oerlemans, 2010), which reduces bare ice albedo and likely introduces increased ablation area albedo variability. Assigning a wider range of MAR albedo values for bare ice (which has been implemented in most recent release of MAR, v3.4) may improve its representation of the distribution of bare ice albedo, but may not necessarily improve its ability to capture the spatial distribution of ablation area albedo. This could potentially be achieved through the inclusion of an explicit representation of dust and sub-grid-scale hydrology in the model.

4.2.3 Discrepancies in accumulation area trends

As noted in section 3.5, there is a discrepancy between the satellite products, in situ data, and model results regarding albedo trends in the accumulation area of the ice sheet. MOD10A1 and MCD43A3 show significant decreases in accumulation area albedo (-0.04 to -0.03 per decade) while MAR v3.2 trends are generally not statistically significant, and in situ trends are generally small (not larger than -0.01 per decade) or not significant.

A possible explanation for this discrepancy is that MODIS trends are negatively biased as a result of declining instrument sensitivity of the MODIS sensors (Wang et al., 2012). In particular, a larger degradation has been observed for the MODIS Terra satellite (Wang et al., 2012). The MCD43A3 product uses data from both the Terra and Aqua satellites, while MOD10A1 only uses data from Terra. This could potentially explain the larger trends for MOD10A1 relative to MCD43A3 (Table 6, Fig. 13). Box et al. (2012) conclude that declining instrument sensitivity does not substantially affect GrIS albedo trends, because they find larger trends in GC-Net data relative to MOD10A1 for 70% of cases where trends are deemed to be significant. We do not find JJA GC-Net trends larger than those of MODIS, except within the ablation area, with high local variability, in contrast to the findings of Box et al. (2012). The analysis performed here is somewhat different from that employed by Box et al.

1 (2012). Differences in trends may result from the fact that here we have focused on trends for
2 the entire JJA period rather than on monthly trends, and calculate trends for 16 day albedo
3 values rather than calculating a monthly albedo from integrated fluxes over a 1-month period,
4 as was done by Box et al. (2012). We also investigated the possibility that the smaller
5 spectral interval of GC-Net data influences trends by comparing MCD43A3 visible vs.
6 shortwave albedo trends, but did not find the trends to be significantly different from each
7 other. We are not able to confirm that the larger trends from MODIS are associated with
8 declining instrument sensitivity, as this analysis is outside the scope of this study. However,
9 the findings of this study seem consistent with this possibility and this is suggested as a topic
10 for future research.

11

12 **5   Conclusions**

13 We have examined spatio-temporal variability and trends in GrIS albedo using in situ
14 measurements, satellite products obtained from MODIS data, and outputs of a regional
15 climate model (MAR v3.2). The results presented here reveal areas of agreement as well as
16 discrepancies between observational and model estimates of GrIS albedo spatio-temporal
17 variability. Examining local measurements, satellite data, and model results concurrently
18 reveals information about the GrIS albedo and potential biases that would not be revealed by
19 examining the observational datasets or model results individually.

20 The results presented here show that albedo varies spatially as a function primarily of surface
21 properties, in particular melting and bare-ice exposure in the ablation area. These factors are
22 also associated with temporal variations in albedo, resulting in high variability in low
23 elevation regions. The differences in variations with latitude indicated by satellite products
24 appear likely to be a function of inaccuracies associated with the products themselves, rather
25 than a record of actual variations in surface albedo, particularly as the two products are
26 derived from the same MODIS sensors.

27 Both satellite products and MAR model outputs (for v2.0 and v3.2) suggest that there is a
28 bimodal distribution of surface albedo within the ablation area of the ice sheet. Based on
29 model results, we infer that this distribution is associated with the presence of two primary
30 surface types within the ablation area, snow and bare ice. The model's inability to capture the
31 full range of low elevation albedo leads to inaccuracies in the representation of spatiotemporal
32 variations in albedo, which can substantially impact the representation of SMB. The MAR

1 version examined here (v3.2) appears to better represent the full range of bare-ice albedo in

2 the ablation area relative to a previous version (v2.0), but a lower minimum bare ice albedo

3 value (as is implemented in the next version of MAR, v3.4), may produce results that are

4 more consistent with observations. Even so, it may be necessary to account for the presence

5 of impurities and sub-grid scale hydrology in order to fully capture spatial variations in

6 albedo.

7 The analysis performed here indicates a statistically significant decrease in ablation area

8 albedo over the period 2000-2013 that is consistent with previous studies (Box et al., 2012;

9 Tedesco et al., 2011, 2013; Stroeve et al., 2013). This decrease is consistent with a coincident

10 decline in ablation area SMB recorded by both models and observations (e.g. Fettweis et al.,

11 2011; Ettema et al., 2009). Our results are inconclusive regarding high elevation trends in

12 albedo; we observe inconsistencies between satellite-derived trends and trends obtained from

13 in situ measurements and MAR v3.2 results. We are therefore unable to confirm previously

14 reported decreases in surface albedo at high elevations.

15 Future research should be directed towards understanding the reasons for discrepancies

16 between satellite products, in situ data and model results, in order to better understand

17 changes in GrIS albedo. This includes resolving discrepancies regarding high-elevation

18 trends, and discrepancies in mean satellite-derived surface albedo at high latitudes. Models

19 such as MAR appear to be effective at capturing surface albedo, but refinements are necessary

20 for representation of surface albedo in low elevation areas. In particular, the representation of

21 bare ice albedo is critical. Sensitivity studies, such as those performed by van Angelen et al.

22 (2012) of the impact of surface albedo on SMB variability, may help to quantify the accuracy

23 with which surface albedo must be modeled for a given region. Analysis of spatiotemporal

24 variations in albedo across different spatial scales (including at a higher spatial resolution than

25 has been examined here) may also become increasingly important as models operate at higher

26 spatial resolutions, and as we seek to understand the GrIS surface mass and energy budget in

27 greater detail. Given the strong relationship between surface albedo and SMB, these future

28 studies are crucial for efforts aiming at estimating and predicting the impact of current and

29 future climate change on GrIS SMB.

30

23

References

Bamber, J.L., Ekholm, S., and Krabill, W.B.: A new, high-resolution digital elevation model of Greenland fully validated with airborne laser altimeter data, J. Geophys. Res., 106, B4, 6733-6745, 2001.

Bamber, J.L., Griggs, J.A., Hurkmans, R.T.W.L., Dowdeswell, J.A., Gogineni, S.P., Howat, I., Mouginot, J., Paden, J., Palmer, S., Rignot, E., and Steinhage, D.: A new bed elevation dataset for Greenland, The Cryosphere, 7, 449-510, doi:10.5194/tc-7-499-2013, 2013.

Bøggild, C. E., Brandt, R. E., Brown, K. J., Warren, S. G.: The ablation zone in northeast Greenland: ice types, albedos and impurities, J. Glaciol., 56, 2010.

Box, J. E. and Rinke, A.: Evaluation of Greenland Ice Sheet surface climate in the HIRHAM Regional Climate Model using automatic weather station data, J. Climate, 16, 1302-1319, 2002.

Box, J.E., Bromwich, D.H., Veenhuis, B.A., Bai, L.-S., Stroeve, J.C., Rogers, J.C., Steffen, K., Haran, T. and Wang, S.-H.: Greenland Ice Sheet surface mass balance variability (1988-2004) from calibrated Polar MM5 output, J. Climate, 19, 2783-2800, 2006.

Box, J.E., Fettweis, X., Stroeve, J.C., Tedesco, M., Hall, D.K., and Steffen, K.: Greenland ice sheet albedo feedback: thermodynamics and atmospheric drivers, The Cryosphere, 6, 821-839, 2012.

Brun, E., David, P., Sudul, M., and Brunot, G.: A numerical model to simulate snow-cover stratigraphy for operational avalanche forecasting, J. Glaciol., 38, 128, 13-22, 1992.

Dee, D. P., Uppala, S. M., Simmons, A. J., et al.: The ERA-Interim reanalysis: configuration and performance of the data assimilation system, Q. J. R. Meteorol. Soc., 137: 553-597, doi: 10.1002/qj.828, 2011.

Dumont, M., Brun, E., Picard, G., Michou, M., Libois, Q., Petit, J-R., Geyer, M., Morin, S., and Josse, B.: Contribution of light-absorbing impurities in snow to Greenland's darkening since 2009, Nature, doi:10.1038/NGEO2180, 2014.

Ettema, J., van den Broeke, M.R., van Meijgaard, E., van de Berg, W.J., Bamber, J.L., Box, J.E., Bales, R.C.: Higher surface mass balance of the Greenland ice sheet revealed by high-resolution climate modeling, Geophys. Res. Lett., 36, L12501, doi:10.1029/2009GL038110, 2009.

Fettweis, X.: Reconstruction of the 1979-2006 Greenland ice sheet surface mass balance using the regional climate model MAR, The Cryosphere, 1, 21-40, doi:10.5194/tc-1-21-2007, 2007.

Fettweis, X., Gallée, H., Lefebre, F., and van Ypersele, J.-P.: Greenland surface mass balance simulated by a regional climate model and comparison with satellite-derived data in 1990-1991, Clim. Dynam., 24, 623-640, 2005.

Fettweis, X., van Ypersele, J.-P., Gallée, H., Lefebre, F., and Lefebvre, W.: The 1979-2005 Greenland ice sheet melt extent from passive microwave data using an improved version of the melt retrieval XPGR algorithm, Geophys. Res. Lett., 34, L05502, doi:10.1029/2006GL028787, 2007.

Fettweis, X., Tedesco, M., van den Broeke, M., and Ettema, J.: Melting trends over the Greenland ice sheet (1958-2009) from spaceborne microwave data and regional climate models, The Cryosphere, 5, 359-375, doi:10.5194/tc-5-359-2011, 2011.

Fettweis, X., Hanna, E., Lang, C., Belleflamme, A., Erpicum, M., and Gallée, H.: *Brief communication* "Important role of the mid-tropospheric atmospheric circulation in the recent surface melt increase over the Greenland ice sheet", The Cryosphere, 7, 241-248, doi:10.5194/tc-7-241-2013, 2013a.

Fettweis, X., Franco, B., Tedesco, M., van Angelen, J. H., Lenaerts, J. T. M., van den Broeke, M. R., and Gallée, H.: Estimating the Greenland ice sheet surface mass balance contribution to future sea level rise using the regional atmospheric climate model MAR, The Cryosphere, 7, 469-489, doi:10.5194/tc-7-469-2013, 2013b.

Franco, B., Fettweis, X., and Erpicum, M.: Impact of spatial resolution on the modelling of the Greenland ice sheet surface mass balance between 1990-2010, using the regional climate model MAR, The Cryosphere, 6, 695-711, doi:10.5194/tc-6-695-2012, 2012.

Gallée, H.: Air-sea interactions over Terra Nova Bay during winter: simulation with a coupled atmosphere-polynya model, J. Geophys. Res., 102, D12, 13835-13849, 1997.

Gallée, H., and Schayes, G.: Development of a three-dimensional meso-γ primitive equation model: katabatic winds simulation in the area of Terra Nova Bay, Antarctica, Mon. Weather Rev., 122, 671-685, 1994.

1 Greuell, W., and Konzelman, T.: Numerical modelling of the energy balance and the englacial

2 temperature of the Greenland Ice Sheet. Calculations for the ETH-Camp location (West

3 Greenland, 1155 m.a.s.l.), Global and Planetary Change, 9, 91-114, 1994.

4 Häkkinen, S., Hall, D. K., Shuman, C. A., Worthen, D. L., and DiGirolamo, N. E.: Greenland

5 ice sheet melt from MODIS and associated atmospheric variability, Geophys. Res. Lett., 41,

6 1600-1607, 2014.

7 Hall, D. K., and Martinec, J.: Remote Sensing of Ice and Snow, Chapman and Hall, London,

8 1985.

9 Hall, D.K., Salomonson, V.V., and Riggs, G.A.: MODIS/Terra Snow Cover Daily L3 Global

10 500 m Grid. Version 5. [Tiles h15v02, h16v02, h17v02, h16v01, h17v02, h16v00, h17v00],

11 National Snow and Ice Data Center, Boulder, Colorado USA, 2012.

12 Konzelmann, T., and Ohmura, A.: Radiative fluxes and their impact on the energy balance of

13 the Greenland ice sheet, J. Glaciol., 41, 490-502, 1995.

14 Klein, A.G., and Stroeve, J.: Development and validation of a snow albedo algorithm for the

15 MODIS instrument, Ann. of Glaciol., 34, 45-52, 2002.

16 Lefebre, F., Gallée, H., van Ypersele, J.-P.: Modeling of snow and ice melt at ETH Camp

17 (West Greenland): a study of surface albedo, J. Geophys. Res., 108, 4231,

18 doi:10.1029/2001JD001160, 2003.

19 Lefebre, F., Fettweis, X., Gallée, H., van Ypersele, J.-P., Marbaix, P., Greuell, W., and

20 Calanca, P.: Evaluation of a high-resolution regional climate model simulation over

21 Greenland, Clim. Dynam., 25, 99-116, doi: 10.1007/s00382-005-0005-8, 2005.

22 Nghiem, S. V., Hall, D. K., Mote, T. L., Tedesco, M., Albert, M. R., Keegan, K., Shuman, C.

23 A., DiGirolamo, N. E., and Neumann, G.: The extreme melt across the Greenland ice sheet in

24 2012, Geophys. Res. Lett., 39, L20502, doi: 10.1029/2012GL053611, 2012.

25 Rae, J. G. L., Aðalgeirsdóttir, G., Edwards, T. L., Fettweis, X., Gregory, J. M., Hewitt, H. T.,

26 Low, J. A., Lucas-Picher, P., Mottram, R. H., Payne, A. J., Ridley, J. K., Shannon, S. R., van

27 de Berg, W. J., van de Wal, R. S. W. and van den Breoke, M. R.: Greenland ice sheet surface

28 mass balance: evaluating simulations and making projections with regional climate models,

29 The Cryosphere, 6, 1275-1294, doi: 10.5194/tc-6-1275-2012, 2012.

1 Rignot, E., Velicogna, I., van den Broeke, M. R., Monaghan, A. and Lenaerts, J.:
2 Acceleration of the contribution of the Greenland and Antarctic ice sheets to sea level rise,
3 Geophys. Res. Lett., 38, L05503, doi: 10.1029/2011GL046583, 2011.

4 Schaaf, C. B., Gao, F., Strahler, A. H., Lucht, W., Li, X., Tsang, T., Strugnell, N. C., Zhang,
5 X., Jin, Y., Muller, J.-P., Lewis, P., Barnsley, M., Hobson, P., Disney, M., Roberts, G.,
6 Dunderdale, M., Doll, C., d'Entremont, R. P., Hu, B., Liang, S., Privette, J. L. and Roy, D.:
7 First operational BRDF, albedo nadir reflectance products from MODIS, Remote Sens.
8 Environ., 83, 135-148, 2002.

9 Schaaf, C.B., Wang, Z., and Strahler, A.H.: Commentary on Wang and Zender – MODIS
10 snow albedo bias at high solar zenith anlges relative to theory and to in situ observations in
11 Greenland, Remote Sens. Environ., 115, 1296-1300, 2011.

12 Steffen, K., Box, J.E., and Abdalati, W.: Greenland Climate Network: GC-Net, in: CRREL
13 96-27 Special report on glaciers, ice sheets and volcanoes, trib. to M. Meier, edited by:
14 Colbeck, S. C., US Army Cold Regions Research and Engineering Laboratory (CRREL),
15 Hanover, New Hampshire, 98-103, 1996.

16 Stroeve, J., Box, J.E., Gao, F., Liang, S., Nolin, A. and Schaaf, C.: Accuracy assessment of
17 the MODIS 16-day albedo product for snow: comparisons with Greenland in situ
18 measurements, Remote Sens. Environ., 94, 46-60, 2005.

19 Stroeve, J.C., Box, J.E. and Haran, T.: Evaluation of the MODIS (MOD10A1) daily snow
20 albedo product over the Greenland ice sheet, Remote Sens. Environ., 105, 155-171, 2006.

21 Stroeve, J.C., Box, J.E., Wang, Z., Schaaf, C., and Barret, A.: Re-evaluation of MODIS
22 MCD43 Greenland albedo accuracy and trends, Remote Sens. Environ., 138, 199-214, 2013.

23 Tedesco, M., and Fettweis, X.: 21st century projections of surface mass balance changes for
24 major drainage systems of the Greenland ice sheet, Environ. Res. Lett., 7, 045050, doi:
25 10.1088/1748-9326/7/4/045405, 2012.

26 Tedesco, M., Serreze, M., and Fettweis, X.: Diagnosing the extreme surface melt event over
27 southwestern Greenland in 2007, The Cryosphere, 2, 159-166, doi: 10.5194/tc-2-159-2008,
28 2008.

29 Tedesco, M., Fettweis, X., van den Broeke, M. R., van de Wal, R. S. W., Smeets, C. J. P. P.,
30 van de Berg, W. J., Serreze, M. C., and Box, J. E.: The role of albedo and accumulation in the

2010 melting record in Greenland, Environ. Res. Lett., 6, 014005, doi:10.1088/1748-9326/6/1/014005, 2011.

Tedesco, M., Alexander, P., Box, J. E., Cappelen, J., Mote, T., Steffen, K., van de Wal, R. S. W., Wahr, J., and Wouters, B.: Greenland Ice Sheet, in: State of the Climate in 2012, edited by: Blunden, J. and Arndt, D., B. Am. Meteorol. Soc., 94, S121-S123, 2013.\

Uppala, S. M., Kållberg, P. W., Simmons, A. J., et al.: The ERA-40 re-analysis, Q. J. R. Meteorol. Soc., 131, 2961-3012, doi: 10.1256/qj.04.176, 2005.

van Angelen, J. H., Lenaerts, J. T. M., Lhermitte, S., Fettweis, X., Kuipers Munneke, P., van den Broeke, M. R., van Meijgaard, E., Smeets, C. J. P. P.: Sensitivity of Greenland Ice Sheet surface mass balance to surface albedo parameterization: a study with a regional climate model, The Cryosphere, 6, 1175-1186, doi: 10.5194/tc-6-1175-2012, 2012.

van den Broeke, M., Bamber, J., Ettema, J., Rignot, E., Schrama, E., Jan van de Berg, W., van Meijgaard, E., Velicogna, I., and Wouters, B.: Partitioning recent Greenland mass loss, Science, 326, 984-986, doi: 10.1126/science.1178176, 2009.

van den Broeke, M. R., Smeets, C. J. P. P., and van de Wal, R. S. W.: The seasonal cycle and interannual variability of surface energy balance and melt in the ablation zone of the west Greenland ice sheet, The Cryosphere, 5, 377-390, doi:10.5194/tc-5-377-2011, 2011.

van de Wal, R. S. W. and Oerlemans, J.: An energy balance model for the Greenland Ice Sheet, Global Planet. Change, 9, 115-131, 1994.

van de Wal, R. S. W., Greuell, W., van den Broeke, M. R., Reijmer, C. H., and Oerlemans, J.: Surface mass-balance observations and automatic weather station data along a transect near Kangerlussuaq, West Greenland, Ann. Glaciol., 42, 311-316, 2005.

van de Wal, R. S. W., Boot, W., Smeets, C. J. P. P., Snellen, H., van den Broeke, M. R., and Oerlemans, J.: Twenty-one years of mass balance observations along the K-Transect, West-Greenland, Earth Syst. Sci. Data, 4, 31-35, doi:10.5194/essd-4-31-2012, 2012.

Vernon, C. L., Bamber, J. L., Box, J. E., van den Broeke, M. R., Fettweis, X., Hanna, E., and Huybrechts, P.: Surface mass balance model intercomparison for the Greenland ice sheet, The Cryosphere, 7, 599-614, doi: 10.5194/tc-7-599-2013, 2013.

Wang, D., Morton, D., Masek, J., Wu, A., Nagol, J., Xiong, X., Levy, R., Vermote, E., and Wolfe, R.: Impact of sensor degradation on the MODIS NDVI time series, Remote Sens. Environ., 119, 55-61, 2012.

Wang, X. and Zender, C. S.: MODIS snow albedo bias at high solar zenith angles relative to theory and to in situ observations in Greenland, Remote Sens. Environ., 114, 563-575, 2009.

Wientjes, I. G. M., and Oerlemans, J.: An explanation for the dark region in the western melt zone of the Greenland ice sheet, The Cryosphere, 4, 261-268, 2010.

Wiscombe, W. J., and Warren, S. G.: A model for the spectral albedo of snow: pure snow, J. Atmos. Sci., 37, 2712-2733, 1980.

Zuo, Z. and Oerlemans, J.: Modelling albedo and specific balance of the Greenland ice sheet: calculations for the Søndre Strømfjord transect, J. Glaciol., 42, 305-317, 1996.

1   **Table 1.** Range of possible albedo values for different surface types in MAR v2.0 and v3.2

	MAR v2.0	MAR v3.2
Bare Ice	0.45	0.45 to 0.55
Firn	0.45 to 0.65	0.55 to 0.65
Snow	>0.65	>0.65

2

1   **Table 2.** GC-Net and K-Transect weather stations used in this study and years of coverage.

Station Name	Coverage Period	Excluded data
Ablation Area		
Swiss Camp (GC-Net)	2000-2003, 2005-2011	2012
JAR 1 (GC-Net)	2000-2012	
JAR 2 (GC-Net)	2000-2005, 2007, 2009-2012	
JAR 3 (GC-Net)	2000-2003	
S5 (K-Transect)	2004-2012	
S6 (K-Transect)	2004-2012	
S9 (K-Transect)	2004-2012	
Peterman ELA (GC-Net)	2012	2003, 2005
Peterman Glacier (GC-Net)	Not Used	2002-2005
Accumulation Area, North of 70°N		
GIST (GC-Net)	2001, 2002, 2006, 2012	
Humboldt (GC-Net)	2002-2005, 2007, 2010-2012	
Summit (GC-Net)	2000-2012	
Tunu N (GC-Net)	2000-2002, 2005-2012	
NASA-E (GC-Net)	2000-2007, 2010-2012	
NEEM (GC-Net)	2006-2012	
NASA-U (GC-Net)	Not Used	2003-2012
NGRIP (GC-Net)	Not Used	2002-2004, 2007-2009
Accumulation Area, South of 70°N		
KULU (GC-Net)	2000	
S10 (K-Transect)	2010-2012	
Crawford Point 1 (GC-Net)	2000-2004	2005-2010
Crawford Point 2 (GC-Net)	2000	
Dye-2 (GC-Net)	2000-2012	
Saddle (GC-Net)	2000-2001, 2003-2008, 2010-2012	
South Dome (GC-Net)	2003-2012	
NASA SE (GC-Net)	2000-2007, 2009-2012	
KAR (GC-Net)	2000, 2001	
Aurora (GC-Net)	Not Used	

2

3

1 **Table 3.** Mean 2000-2012 JJA Greenland ice sheet albedo, for MOD10A1, MCD43A3 BSA

2 shortwave, and MAR clear-sky albedo, averaged within the mass balance areas shown in Fig.

3 1 and Table 2. Only good quality MODIS data are used here. All data have been averaged

4 over the same 16 day periods of the MCD43A3 product. Only periods when coincident data

5 for all datasets are available have been included.

Locations	MOD10A1	MCD43A3 BSA Shortwave	MAR Clear Sky
Ice-Sheet wide	0.77 ± 0.04	0.73 ± 0.04	0.75 ± 0.03
Ablation Area	0.68 ± 0.07	0.63 ± 0.07	0.68 ± 0.07
Accumulation Area	0.80 ± 0.03	0.75 ± 0.03	0.77 ± 0.02
Acc. Area (N. of 70°N)	0.80 ± 0.03	0.75 ± 0.03	0.77 ± 0.02
Acc. Area (S. of 70°N)	0.78 ± 0.03	0.77 ± 0.03	0.77 ± 0.02

6

7

Table 4. Same as Table 3, but for the average of 16 day data for all in situ stations within each region.

Locations	MOD10A1	MCD43A3 BSA Shortwave	MAR Cloud-Corrected	In Situ
All stations	0.69 ± 0.06	0.67 ± 0.04	0.70 ± 0.04	0.74 ± 0.05
Ablation Area	0.51 ± 0.09	0.50 ± 0.07	0.57 ± 0.06	0.56 ± 0.08
AccumulationArea	0.79 ± 0.04	0.77 ± 0.02	0.76 ± 0.02	0.82 ± 0.03
Acc. Area (N. of 70°N)	0.82 ± 0.04	0.75 ± 0.02	0.78 ± 0.01	0.83 ± 0.02
Acc. Area (S. of 70°N)	0.77 ± 0.04	0.78 ± 0.03	0.75 ± 0.03	0.81 ± 0.03

1 **Table 5.** Mean and standard deviation for the best fit to the distributions of ablation area
2 albedo shown in Fig. 12 (assuming that the appropriate distribution is a combination of two
3 normal distributions).

	MOD10A1	MCD43A3 BSA Shortwave	MAR v2.0 Cloud-Corrected	MAR v3.2 Cloud-Corrected
First Mode (Ice)	0.57 ± 0.10	0.55 ± 0.10	0.50 ± 0.05	0.61 ± 0.06
Second Mode (Snow)	0.73 ± 0.06	0.71 ± 0.04	0.74 ± 0.04	0.74 ± 0.03

4

1   **Table 6.** Trends (and 95% confidence intervals) in JJA albedo (fraction per decade) at GC-
2   Net and K-Transect weather stations and the nearest MOD10A1, MCD43A3, and MAR
3   pixels. In this case, MODIS data flagged as "other quality" have been included. Only 16 day
4   periods when coincident estimates are available for all datasets have been used. Values in
5   bold indicate trends significant at the 95% confidence level.

	Period	MCD43A3 BSA Shortwave	MOD10A1	MAR clear-sky	In Situ
Ablation Zone					
Swiss Camp (GC)	2000-2011	**-0.15** ± 0.05	**-0.15** ± 0.06	**-0.05** ± 0.03	**-0.06** ± 0.03
JAR 1 (GC-Net)	2000-2012	**-0.19** ± 0.06	**-0.21** ± 0.07	**-0.07** ± 0.03	**-0.22** ± 0.03
JAR 2 (GC-Net)	2000-2012	**-0.06** ± 0.02	**-0.08** ± 0.03	**-0.04** ± 0.02	<0.01 ± 0.02
S5 (K-Transect)	2004-2012	**-0.05** ± 0.03	**-0.09** ± 0.04	-0.04 ± 0.04	**-0.08** ± 0.04
S6 (K-Transect)	2004-2012	**-0.13** ± 0.07	**-0.19** ± 0.08	**-0.08** ± 0.06	**-0.14** ± 0.06
S9 (K-Transect)	2004-2012	**-0.15** ± 0.05	**-0.17** ± 0.06	**-0.12** ± 0.05	**-0.25** ± 0.05
Accumulation Zone, North of 70°N					
Humboldt (GC)	2002-2011	-0.01 ± 0.02	**-0.05** ± 0.02	**-0.02** ± 0.01	<0.01 ± 0.01
Summit (GC-Net)	2000-2012	**-0.02** ± 0.02	**-0.04** ± 0.02	**<0.01** ± <0.01	<0.01 ± < 0.01
Tunu N (GC-Net)	2000-2012	**-0.03** ± 0.01	**-0.05** ± 0.02	-0.01 ± 0.01	<0.01 ± 0.01
NASA-E (GC-Net)	2000-2011	**-0.02** ± 0.01	**-0.05** ± 0.02	<0.01 ± 0.01	**-0.03** ± 0.01
Accumulation Zone, South of 70°N					
Dye-2 (GC-Net)	2000-2012	**-0.05** ± 0.01	**-0.07** ± 0.02	**-0.01** ± 0.01	-0.01 ± 0.01
Saddle (GC-Net)	2000-2012	**-0.03** ± 0.01	**-0.05** ± 0.02	**-0.01** ± 0.01	-0.01 ± 0.01
South Dome (GC)	2003-2012	**-0.04** ± 0.01	**-0.06** ± 0.02	-0.01 ± 0.01	**-0.08** ± 0.01
NASA SE (GC)	2000-2012	**-0.04** ± 0.01	**-0.07** ± 0.02	**-0.02** ± 0.01	<0.01 ± 0.01

6

7

8
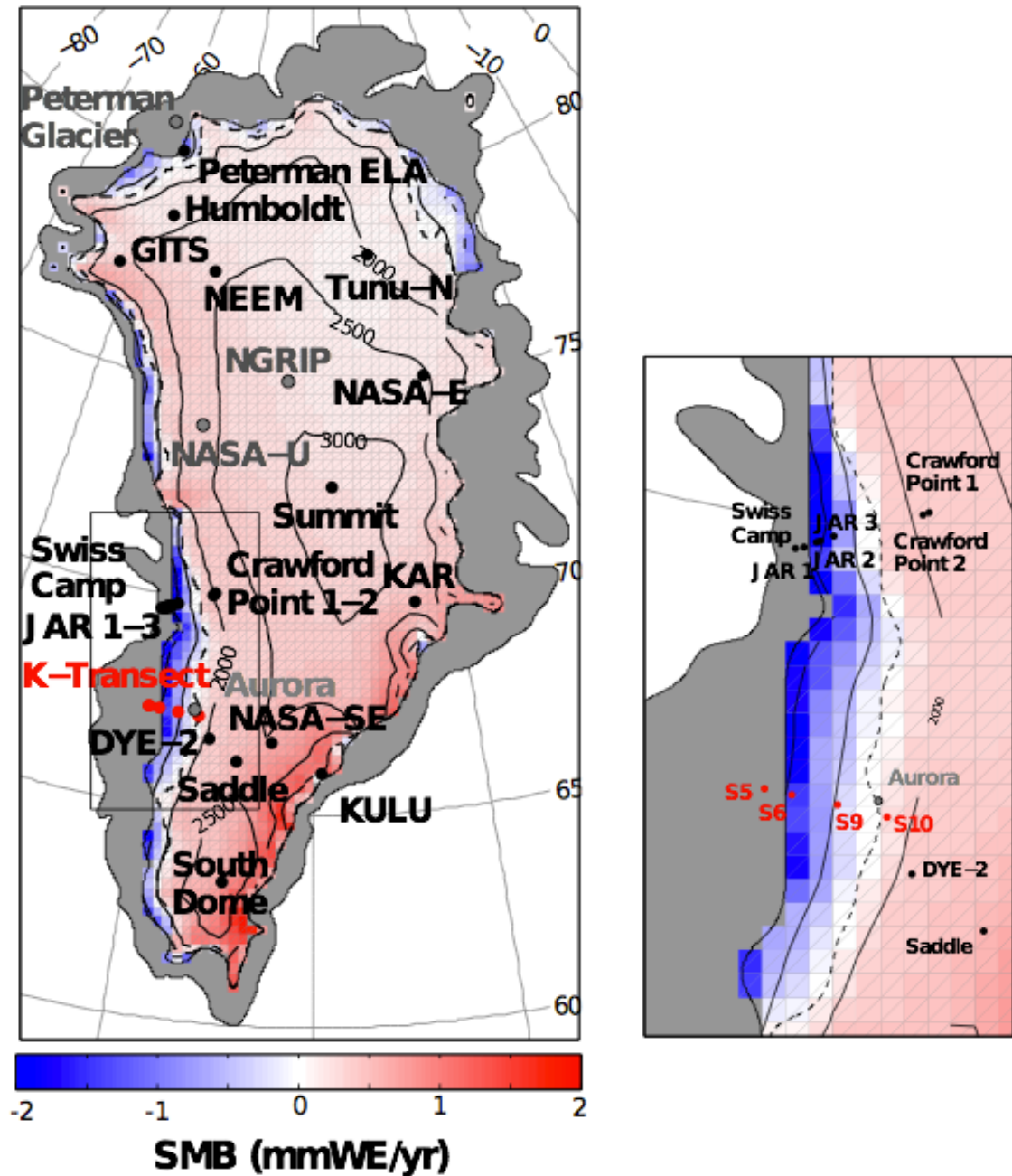
Figure 1. MAR v3.2 mean September 2000 - August 2013 SMB (mWE/yr) and locations of all GC-Net and K-Transect weather stations. Pixels not defined as 100% ice covered in MAR are masked out. The bold dotted black line shows the mean equilibrium line (where the mean SMB is 0). The K-transect stations (S5, S6, S9, S10) are colored red, while GC-Net stations are black. Stations in grey are GC-Net stations that have not been used in this study. Other contour lines indicate elevation in meters above sea level. The inset shows individual stations near the west coast ablation zone.
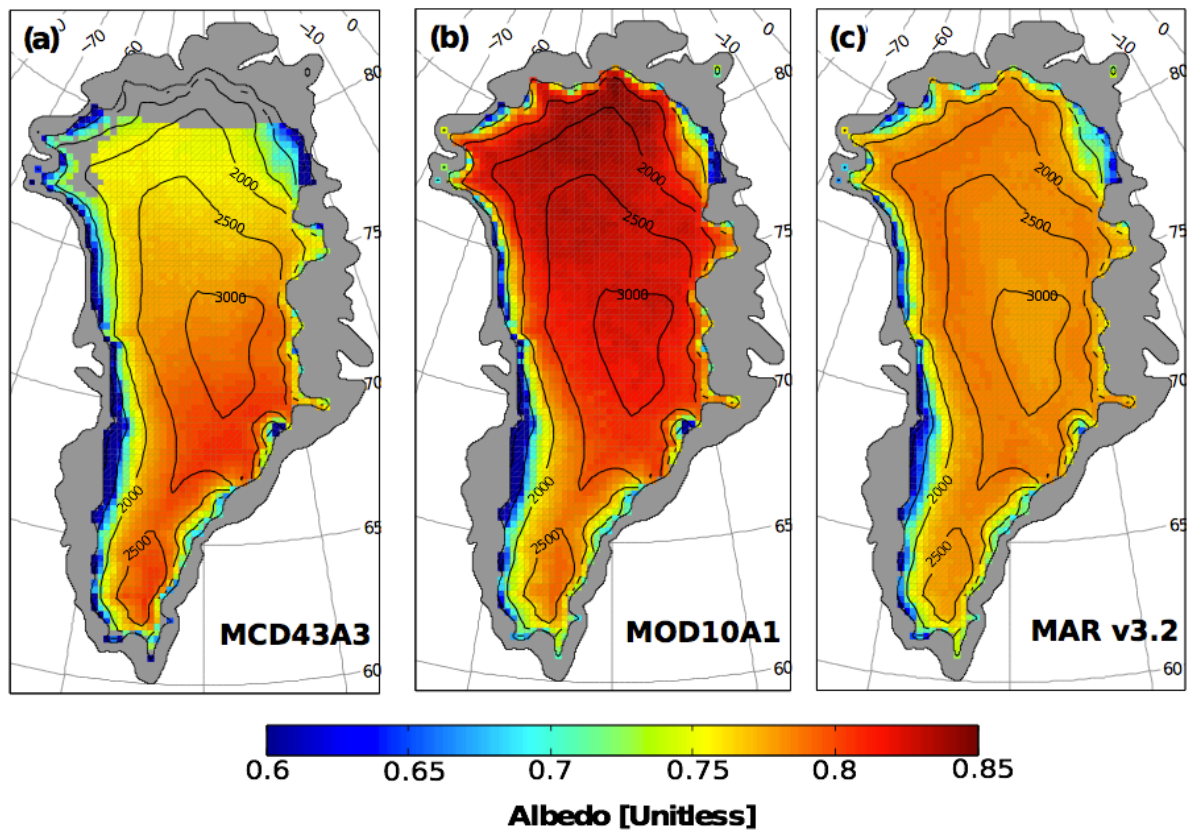
Figure 2. Mean 2000-2013 June, July, August (JJA) albedo (unitless) for **(a)** the MCD43A3 BSA shortwave product (on the MAR grid) **(b)** MOD10A1 product (on the MAR grid), and **(c)** MAR v3.2 clear-sky albedo. Only good quality data MODIS data are used here.
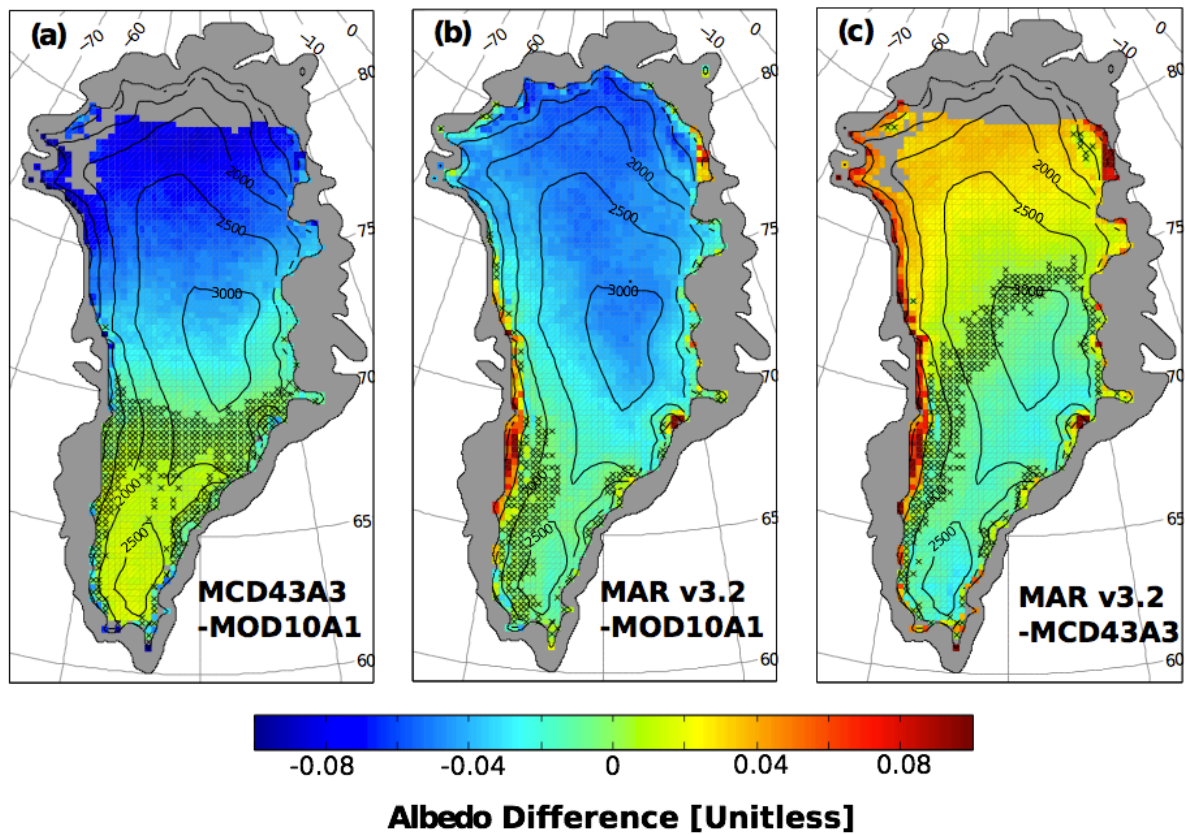
Figure 3. Mean difference in JJA albedo (unitless) for the 2000-2013 period: **(a)** MCD43A3 BSA shortwave minus MOD10A1 **(b)** MAR v3.2 clear-sky minus MOD10A1, and **(c)** MAR v3.2 clear-sky minus MCD43A3. In each case, only coincident data for each of the two datasets being compared is used. MAR grid boxes where the difference is not statistically significant at the 95% confidence level are marked with a grey "x".

1

2
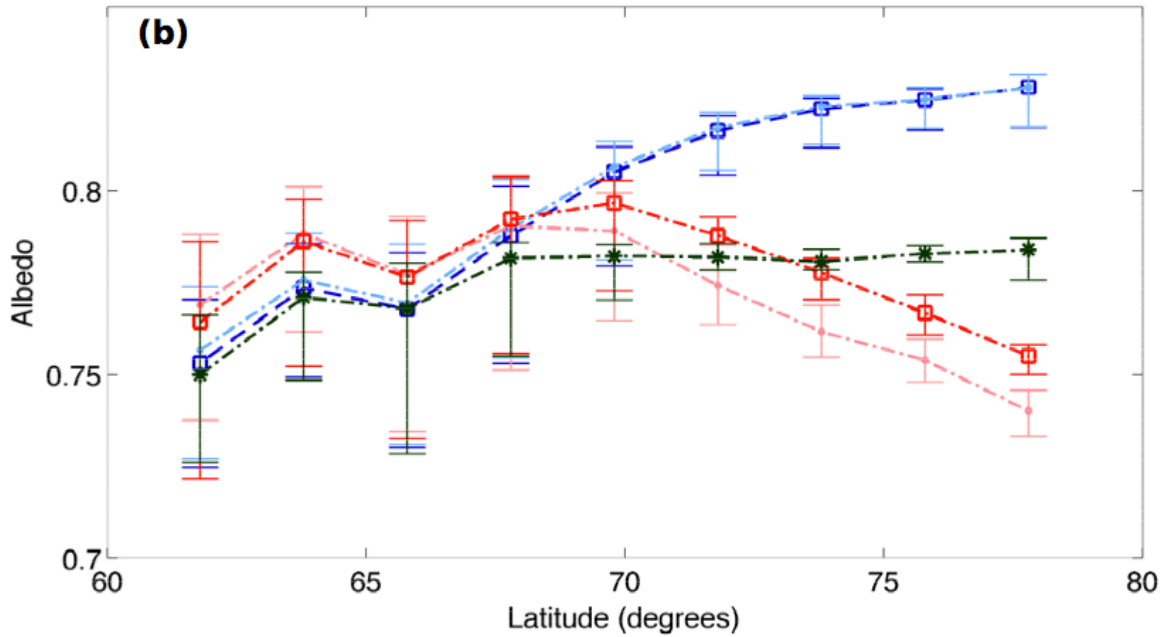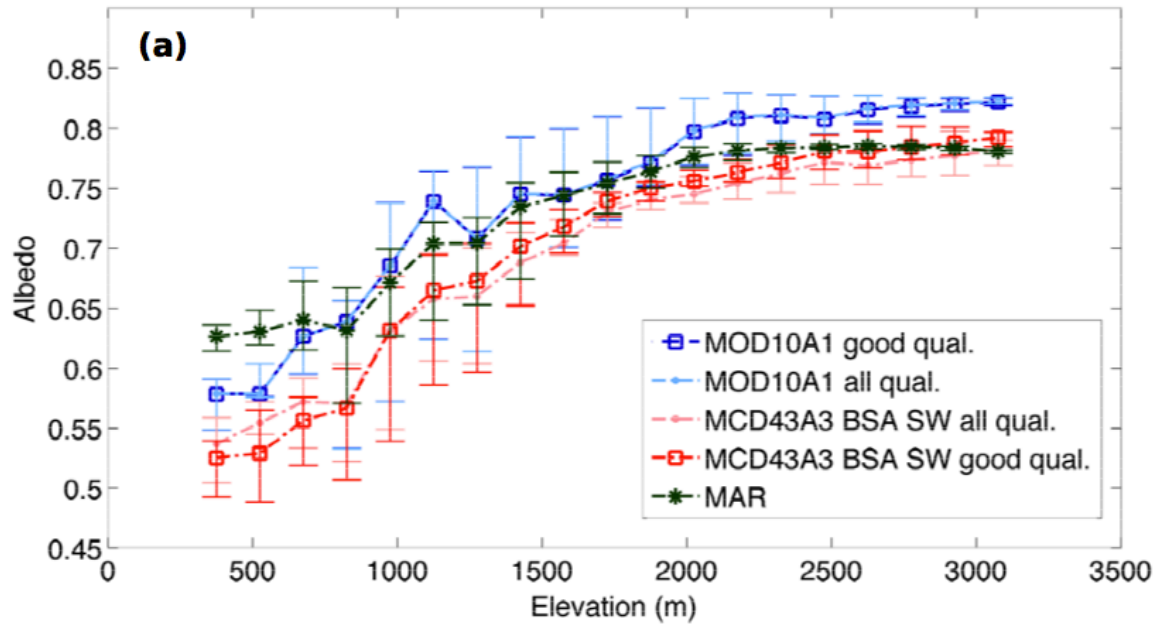
3 **Figure 4. (a)** Mean 2000-2013 JJA MOD10A1, MCD43A3 BSA shortwave (SW), and MAR

4 v3.2 clear sky GrIS albedo (unitless) as a function of elevation divided into 150 m elevation

5 bands. Error bars indicate standard deviation within each elevation band. **(b)** The same as **(a)**

6 but for albedo as a function of latitude, divided into 2° Latitude bands. "Good qual."

7 indicates results obtained by only using "good quality" MODIS data. "All qual." indicates

8 that all available MODIS observations have been used.

9

1

2
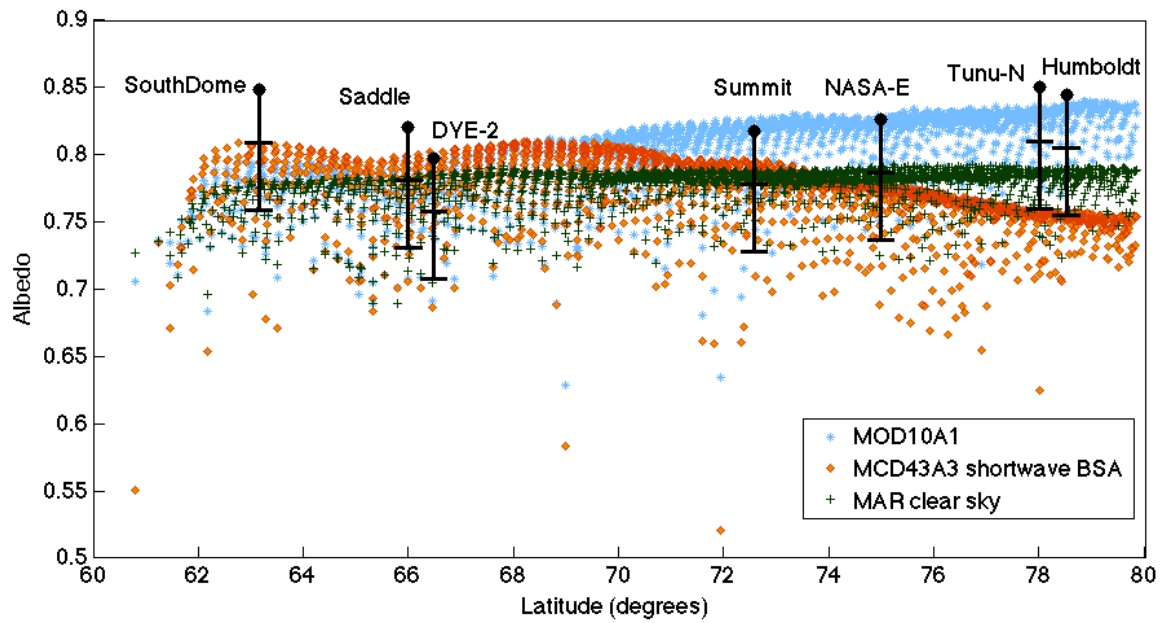
3 **Figure 5.** 2000-2012 mean JJA albedo (unitless) for the MAR accumulation zone vs. latitude,

4 for MOD10A1, MCD43A3 BSA shortwave, MAR v3.2 clear-sky, and GC-Net station data

5 (black circles) for stations with a record spanning at least 7 years of the 2000-2012 period.

6 Only MODIS data flagged as "good quality" are used here.   The error bars for GC-Net

7 stations indicate the range of corrections to GC-Net data (between 0.04 and 0.09) employed

8 by Stroeve et al. (2005).

9
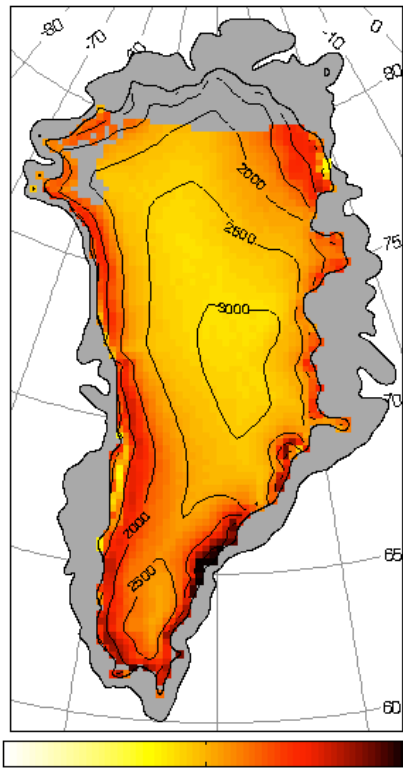
Figure 6. MCD43A3 BSA visible (0.3–0.7 μm) minus MCD43A3 BSA shortwave (0.3–5 μm) 2000-2013 JJA mean albedo (unitless) on the MAR grid. Areas not defined as 100% ice covered in MAR v3.2 are excluded.

1
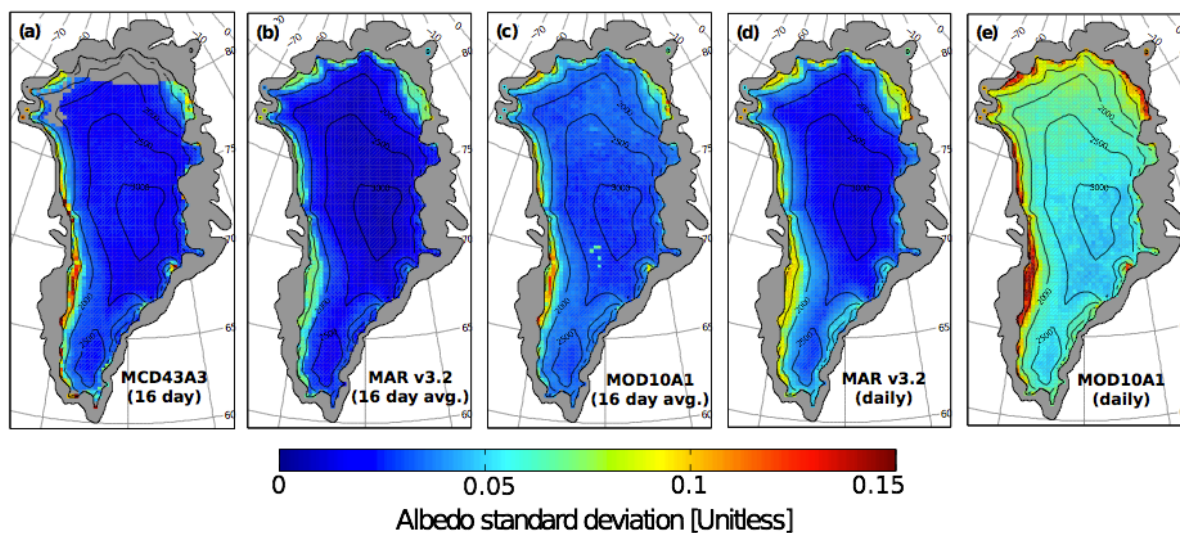
2 **Figure 7.** Standard deviation of JJA albedo (unitless) (2000-2013) for **(a)** MCD43A3
3 shortwave BSA **(b)** MAR v3.2 clear sky 16 day averages **(c)** MOD10A1 16 day averages **(d)**
4 MAR v3.2 clear sky daily, and **(e)** MOD10A1 daily.
5
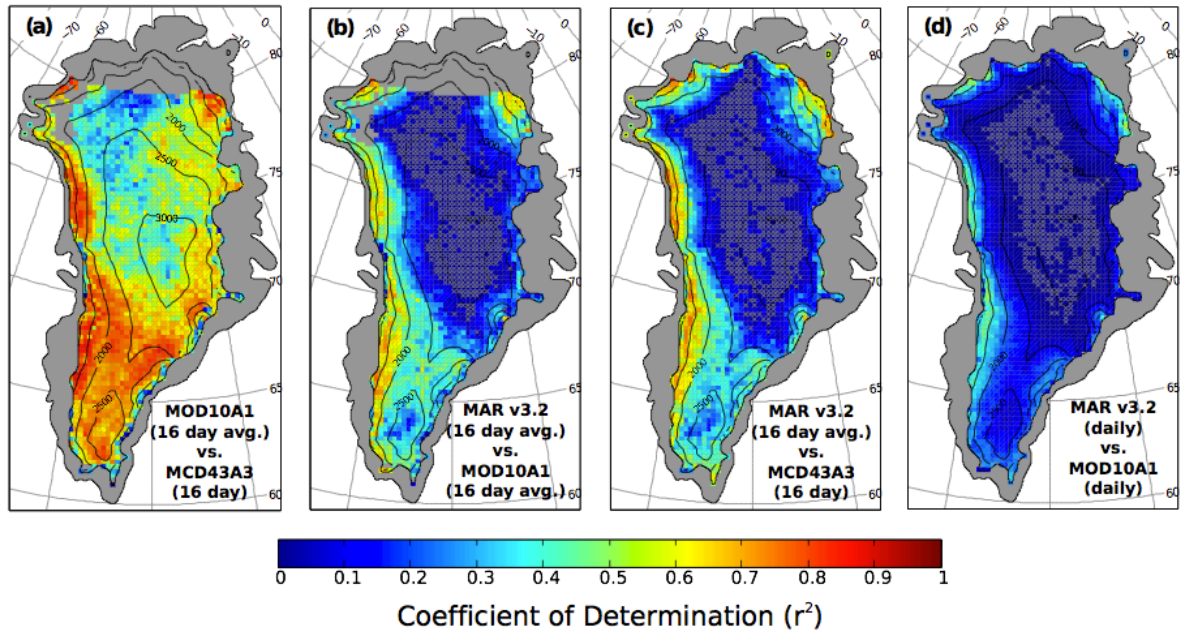
Figure 8. Coefficients of determination (r^2 values) for the 2000-2013 period during JJA for **(a)** MOD10A1 (averaged to 16 day periods) vs. MCD43A3 BSA shortwave **(b)** MAR v3.2 clear sky (16 day data) vs. MCD43A3 BSA shortwave, **(c)** MAR v3.2 clear sky (16 day data) vs. MOD10A1 (16 day data), and **(d)** MAR v3.2 clear sky (daily) vs. MOD10A1 (daily). MAR grid boxes where the correlation is not statistically significant are marked with a grey "x".
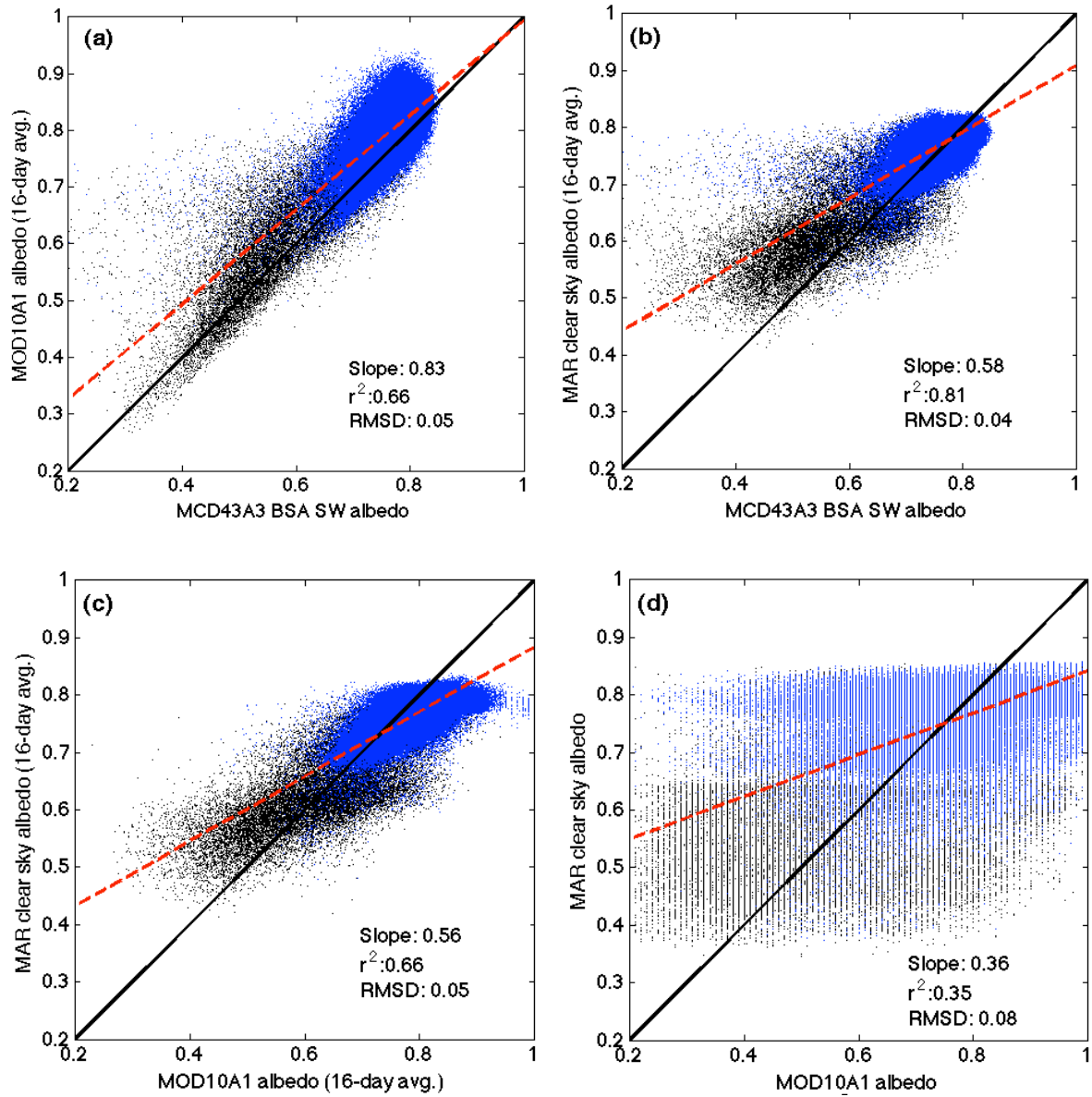
Figure 9. Scatter plots for 2000-2013 JJA albedo for **(a)** MOD10A1 (16 day averaged) vs. MCD43A3 BSA shortwave albedo (unitless) **(b)** MAR v3.2 clear-sky (16 day) vs. MCD43A3 BSA shortwave albedo, **(c)** MAR v3.2 clear-sky (16 day) vs. MOD10A1 (16 day) albedo, and **(d)** MAR v3.2 clear-sky vs. MOD10A1 (daily) albedo. Black points indicate ablation zone locations, while blue points indicate locations within the accumulation zone as defined using MAR v3.2.   A solid black line indicates the 1 : 1 line, and dashed red lines indicate the best linear fit.

1

2

3
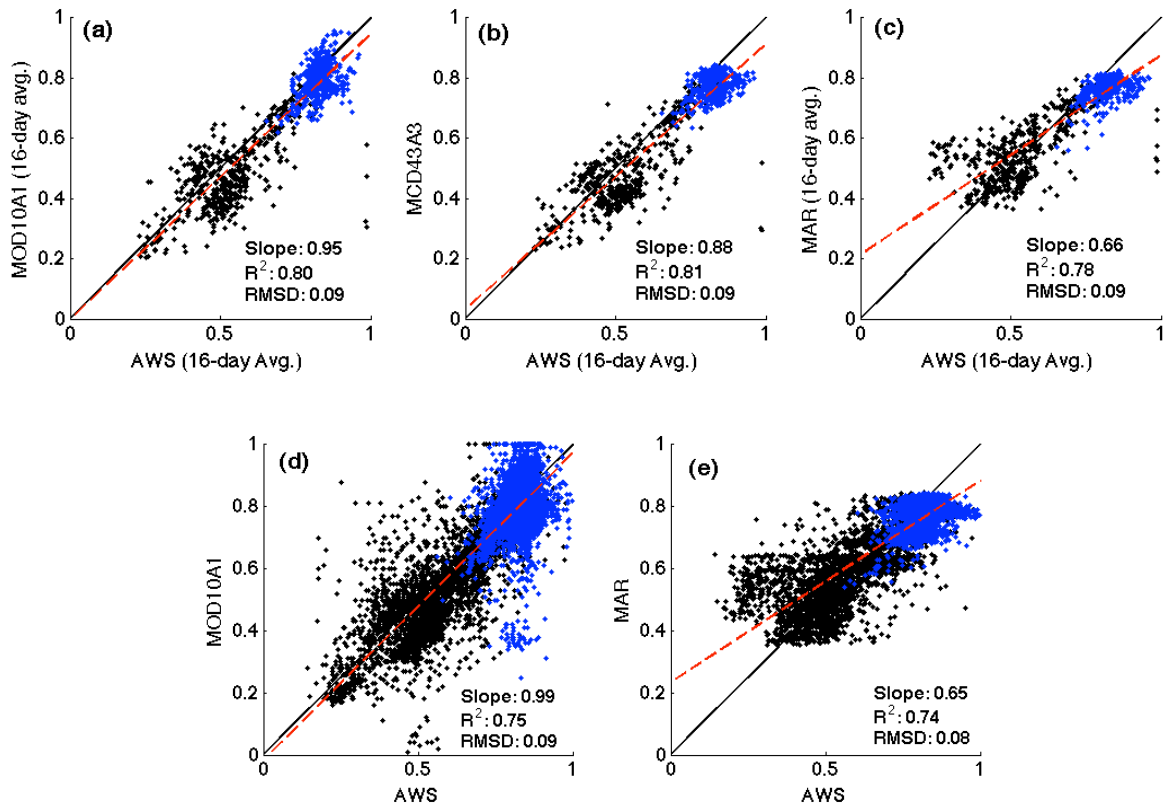
Figure 10. Scatter plots of 2000-2012 JJA mean albedo [unitless] vs. automatic weather station (GC-Net and K-Transect) albedo: **(a)** MOD10A1 16 day averages vs. 16 day in situ **(b)** MCD43A3 BSA shortwave vs. 16 day in-situ **(c)** MAR v3.2 clear sky 16 day vs. 16 day in situ **(d)** MOD10A1 vs. in situ (daily) and **(e)** MAR v3.2 vs. in situ (daily). As for Fig. 9, blue points indicate locations within the accumulation zone as defined using MAR v3.2.
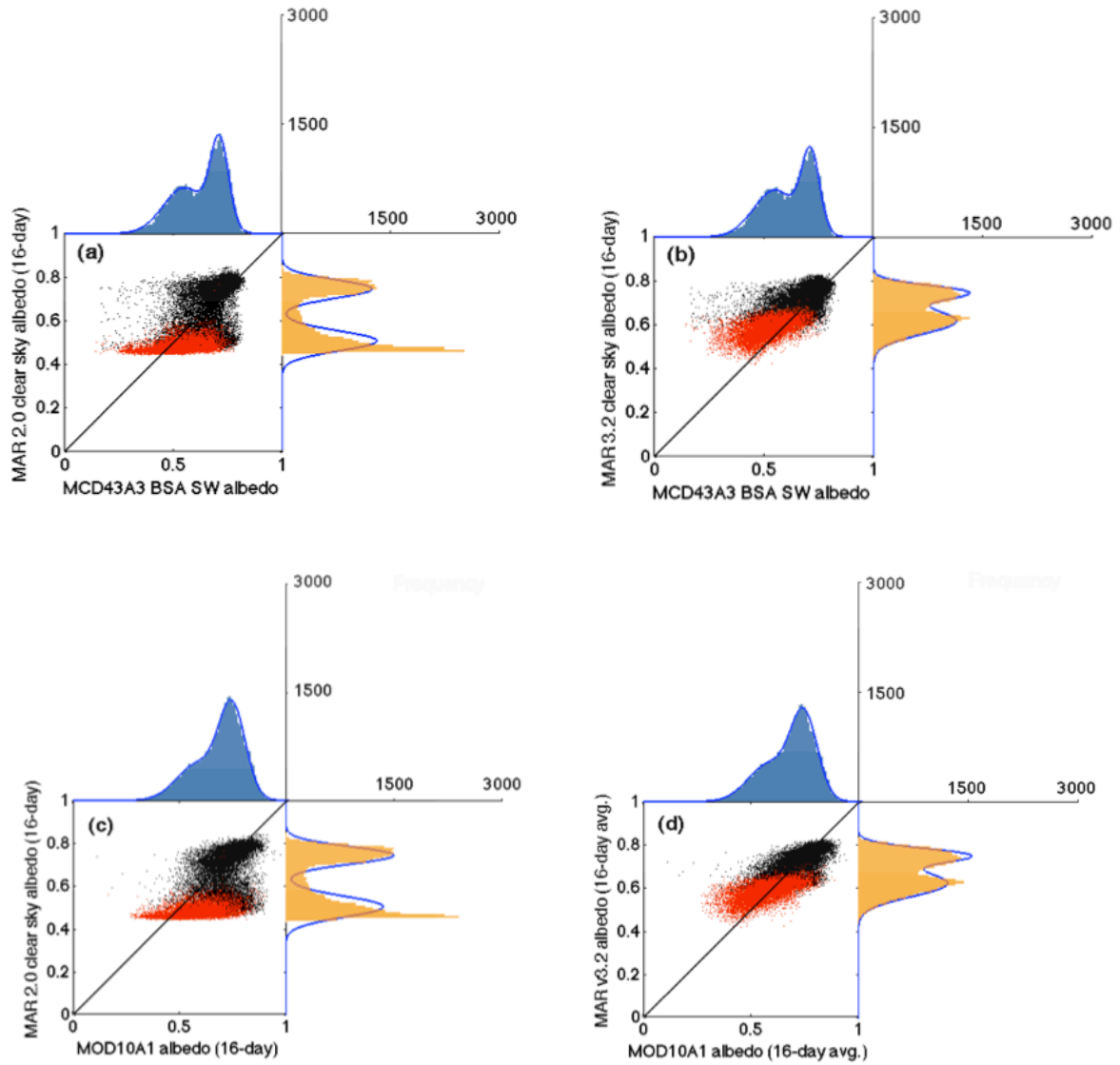
9

10

Figure 11. Scatter plots and histograms for JJA 2000-2012 albedo [unitless] within the MAR v3.2-defined GrIS ablation zone, for **(a)** MAR v2.0 clear sky (16 day avg.) vs. MCD43A3 BSA shortwave. **(b)** The same as **(a)**, but for MAR v3.2. **(c)** The same as **(a)** but for MOD10A1 albedo (averaged to 16 day periods). **(d)** The same as **(c)** but for MAR v3.2. Points where there is snow or firn (surface snowpack density > 830 kg/m^3) for more than 8 days of a 16 day period are shown in red. Light blue curves show the best fit to each distribution obtained using maximum likelihood estimation.
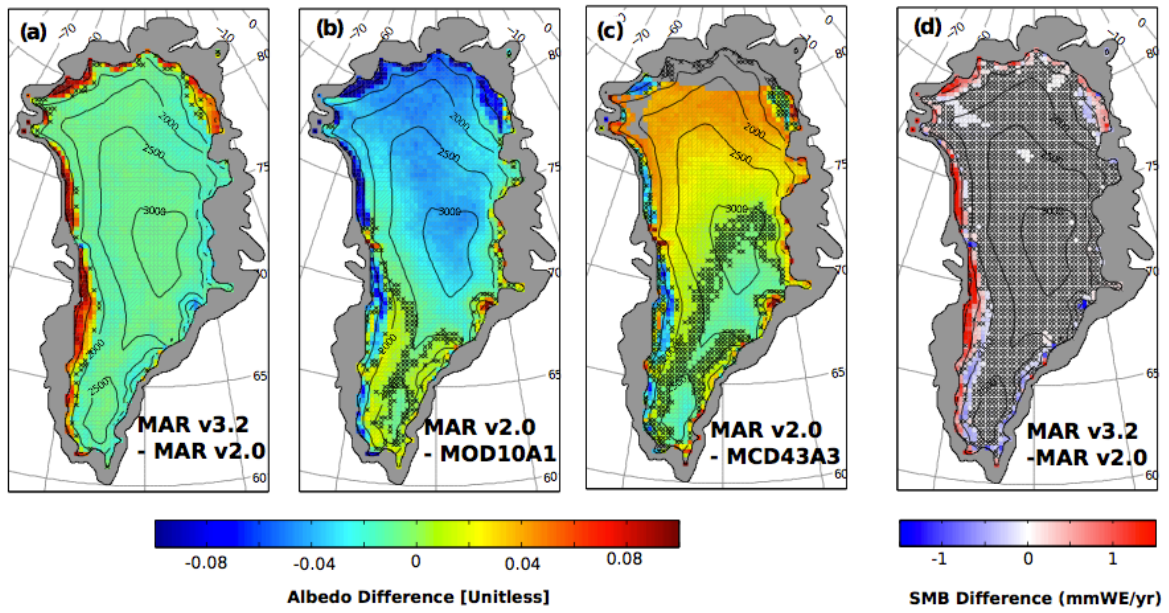
Figure 12. (a) MAR v3.2 clear-sky minus MAR v2.0 clear-sky mean JJA albedo **(b)** MAR clear-sky v2.0 minus MOD10A1 2000-2012 mean JJA albedo, **(c)** MAR clear-sky v2.0 minus MCD43A3 BSA shortwave 2000-2012 mean JJA albedo, and **(d)** MAR v3.2 minus MAR v2.0 mean JJA SMB (mWE/yr) for the same period. Note that in the ablation area, where net SMB is negative (Fig. 1), a positive SMB bias indicates a net mass loss that is reduced in magnitude. Grid boxes where differences are not significant at the 95% confidence level are marked with a black "x".
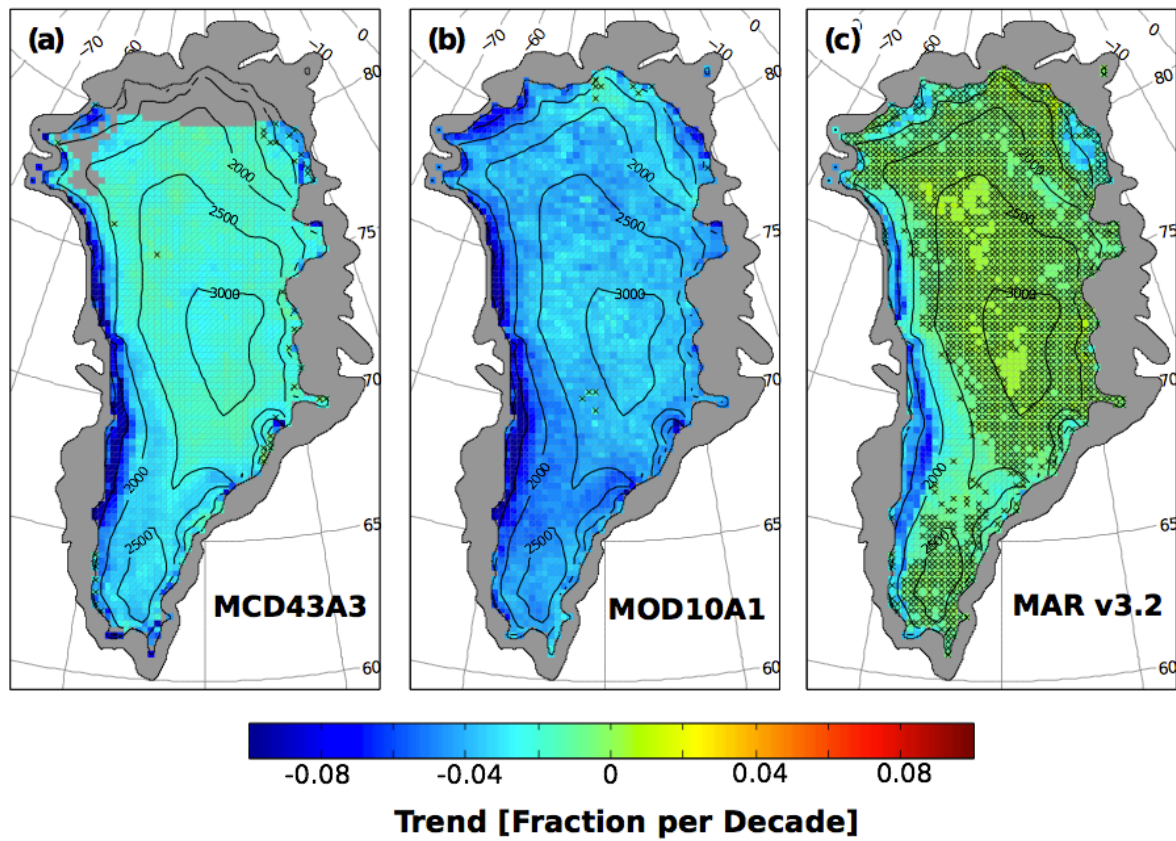
1

2 **Figure 13.** JJA mean albedo trends (2000-2013) in units of fraction per decade for **(a)**
3 MCD43A3 BSA shortwave albedo, **(b)** MOD10A1 albedo, and **(c)** MAR clear-sky albedo.
4 Grid boxes where trends are not significant at the 95% confidence level are marked with a
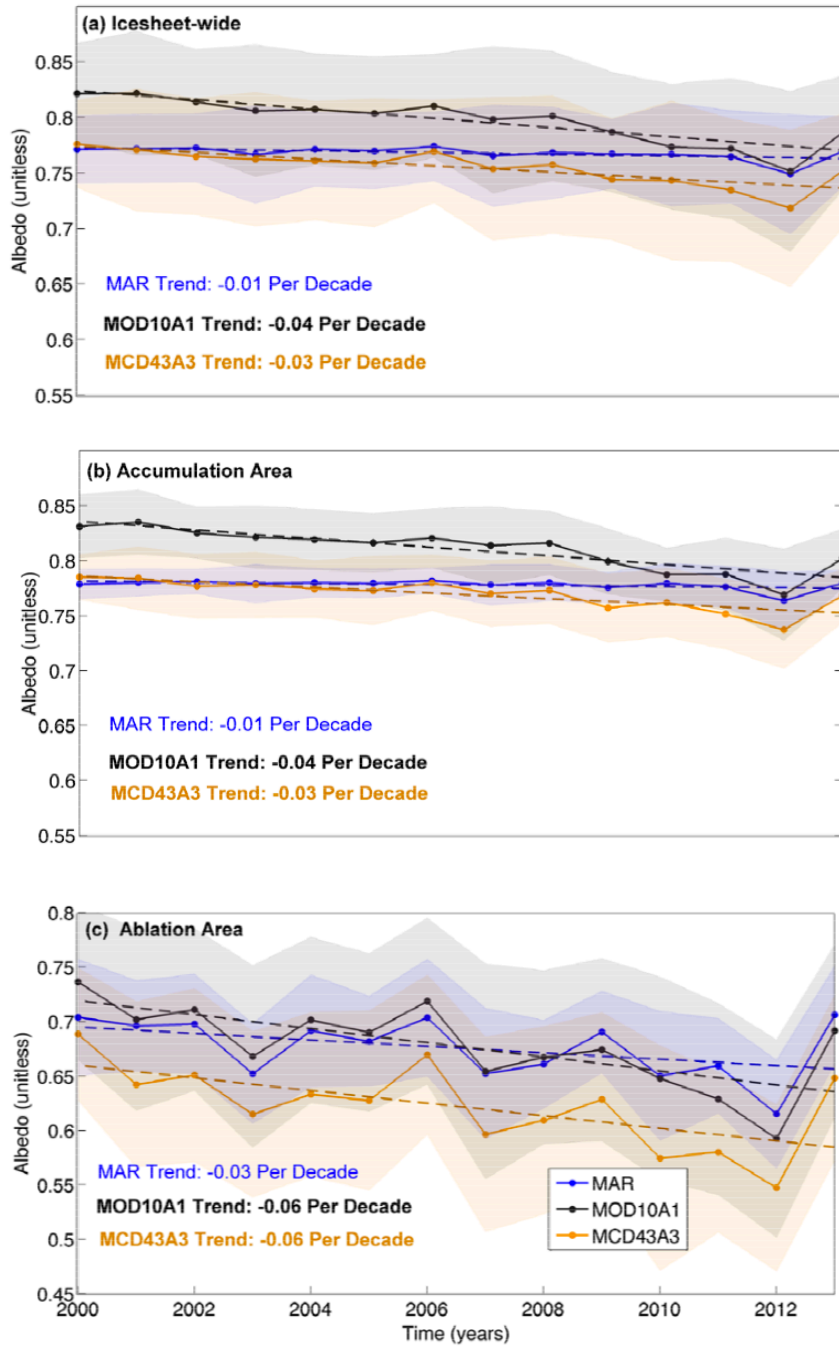5 black "x".

6

Figure 14. Mean annual JJA ice sheet albedo (solid lines) simulated by MAR v3.2 (clear-sky) (blue), MOD10A1 (black) and MCD43A3 BSA shortwave (orange) for 2000-2013 and best linear fit (dashed lines) for **(a)** the entire ice sheet, **(b)** the accumulation zone, and **(c)** the ablation zone defined with MAR v3.2. The trends shown are statistically significant at the 95% confidence level for the MODIS products, but are not statistically significant for MAR. Shaded areas show annual JJA standard deviation of albedo for 16 day periods from each dataset. Note that the y-axis interval is the same for all graphs, but is shifted by 0.1 for **(c)**.